THESIS APPROVAL

The abstract and thesis of Heather Rose Easterly for the Master of Science in Geology were presented October 13, 2005, and accepted by the thesis committee and the department.

COMMITTEE APPROVALS:

_____
Curt D. Peterson, Chair

_____
Georg H. Grathoff

_____
John E. Baham

_____
William Fish
Representative of the Office of Graduate Studies

DEPARTMENTAL APPROVAL:

_____
Michael L. Cummings, Chair
Department of Geology

CHARACTERIZATION OF IRON-BEARING FILMS FOUND ON EPHEMERAL POOLS, CENTRAL COAST, OREGON

by

HEATHER ROSE EASTERLY

A thesis submitted in partial fulfillment of the
requirements for the degree of

MASTER OF SCIENCE
in
GEOLOGY

Portland State University
2005

ABSTRACT

An abstract of the thesis of Heather Rose Easterly for the Master of Science in Geology presented October 13, 2005.

Title: Characterization of Iron-Bearing Films Found on Ephemeral Pools, Central Coast, Oregon

Iron-bearing films have been documented worldwide, but with little characterization or explanation of their formation. Along the Oregon coast the films are found on ephemeral surface pools where ferrous iron discharges from the groundwater. Example sites occur at the base of Pleistocene sand dunes at Seal Rock State Park and Driftwood Creek Wayside. At these pools the iron oxidizes and a thin film of about 300 nm forms. The films have been named Schwimmeisen.

The major constituents of Schwimmeisen are iron and silica in a 3:1 ratio based on scanning electron microscopy – energy dispersive x-ray spectroscopy (SEM-EDS). Schwimmeisen from Seal Rock have higher concentrations of chlorine and sodium, likely due to increased sea-spray. Fourier transfer infrared (FTIR) spectroscopy indicates OH bonds, carbon peaks and peaks similar to ferrihydrite. X-ray diffraction (XRD) and transmission electron microscopy (TEM) show patterns similar to two-line ferrihydrite, with lines around 2.6 Å and 1.5 Å. A third line at 4.5 Å is also present in some areas. Halite and quartz are also found in

association with Schwimmeisen. HRSEM-EDS of the film and flocculent find that carbon is more concentrated in the flocculent. Colorimetric testing finds Schwimmeisen has some mixed valence, roughly 1:5 Fe(II) to Fe(III). Atomic emission spectrometry (AES) and ion chromatography (IC) analysis of the pool water finds concentrations of reduced iron to be 9 ppm, silica 7 ppm, sodium 60 ppm, and chlorine 85 ppm. The average pH was between 5 and 6.

Optical microscopy and SEM find no bacteria in Schwimmeisen or in the water of the pools. High resolution scanning electron microscopy (HRSEM) indicates that there may be iron-oxidizing bacteria in the flocculent on the films. Due to the absence of bacteria directly attached to the films I conclude they are abiotically formed through oxidation at the air-water interface. As oxidation continues the bacteria may attach to the oxidizing film, which falls to the bottom of the seep pool when oxidation is complete. Schwimmeisen form where iron and silica in reducing groundwater are exposed to oxidizing conditions in surface pools and seeps.

ACKNOWLEDGEMENTS

Thank you to my advisor, Georg Grathoff, for his guidance and support throughout this entire process. I would also like to thank John Baham, Nick Chambers, Ann and Larrie Easterly, Rick Hugo, Eric Nielsen, Niki Parenteau, Ben Perkins, and Curt Peterson for their help in the field and in the lab; and Paul Gassman of Environmental Molecular Science Laboratory of Pacific Northwest National Laboratories for work on the FTIR. Funding for this research was provided by the Oregon Society of Soil Scientists, a Portland State University Faculty Enhancement Grant, and by the NOAA office of Sea Grant and Extramural Programs, U.S. Department of Commerce, under grant number NA76RG0476, project number R/SD-04, and by appropriations made by Oregon Legislature.

TABLE OF CONTENTS

LIST OF TABLES

LIST OF FIGURES

INTRODUCTION

Along the Oregon Coast groundwater redistributes iron oxides in the Pleistocene and Holocene sand dunes (Peterson and Hart, 2003). Iron-bearing films form on the surface of ephemeral pools created where Fe(II) rich groundwater exits the dunes. Iridescent and oily in appearance these films break into platelets when physically disturbed. The sandy bottom of these pools is covered in iron particles, called flocculent, as well as organic debris such as leaves and sticks. Johnson (2003) identified two-line-ferrihydrite in a flocculent below the films; however the chemical and mineralogical composition of the film itself was not characterized.

Soluble iron is abundant in some coastal dune systems. In such systems coastal groundwater often has iron levels above 0.3 ppm, requiring treatment to prevent damage to infrastructures (Frank, 1970). Such levels have been found in Coos Bay, Oregon (Magartitz and Luzier, 1985), Long Beach, Washington (Thomas, 1995), and South Wales, Australia (Acworth et al., 1998). Coastal groundwater systems with high iron content feed oceanic ecosystems. Iron regulates biomass and structure growth and thus may act as a limiting nutrient in some marine systems (Johnson et al., 2002).

Despite the importance of iron in coastal dune systems little information is available regarding its diagenesis. Emerson and Weiss (2004) characterize a microbial iron cycle, while Loeppert and Inskeep (1996) summarize the principle forms of iron in the soil. To better constrain the methods of formation, new forms of iron must be characterized. Two-line ferrihydrite is widespread and forms in a variety of

environmental settings, some better known than others. Previous studies have identified ferrihydrite in naturally occurring environments including river systems in Canada (Konhauser and Ferris, 1997), ferri-ferrous streams in Germany (Schwertmann and Friedl,1998), in biofilms in Japan (Tazaki et. al, 2002), and in groundwater outwash in Iceland and New Zealand (Cornell and Schwertmann, 2003). Further characterization of ferrihydrite formation will help to better understand the diagenetic origins of the mineral. Locally, studies of the Pleistocene and Holocene sand dunes along the central Oregon coast indicate that the iron oxides that are present as intergrain cements are primarily hematite, two-line ferrihydrite, and goethite (Grathoff et al., 2003). This study characterizes the surficial iron in the groundwater of the central coastal system of Oregon (Figure 1).

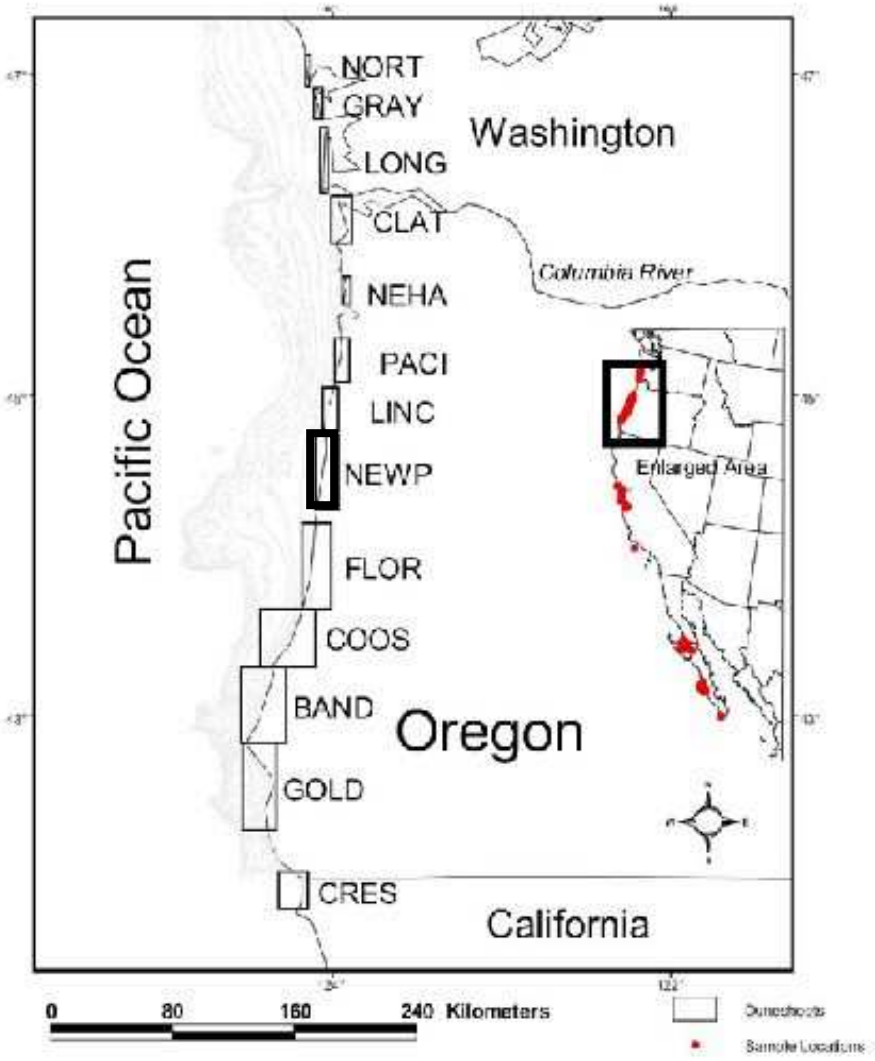

Figure 1. Location of sand dune sheets along the Oregon coast (Peterson et al., 2005). This study concentrates on the Newport dune sheet, outlined in bold.

In this thesis the characteristic morphology, mineralogy, and chemistry of the iron-bearing surface films in coastal dune seeps are presented. Specific seeps were selected based upon the characteristic red-orange two-line ferrihydrite precipitation in pools at the base of sea cliffs. The films were sampled by several methods designed to minimize physical or chemical disturbances. Samples were analyzed by x-ray

diffraction (XRD), scanning electron microscopy (SEM), high-resolution transmission electron microscopy (HRTEM), thermogravimetric analysis (TGA), Fourier transfer infrared (FTIR) spectroscopy, and optical microscopy. Results from these analyses are used to identify the mineral and elemental composition of the surface films. Additional observations distinguish between abiotic and biotic origins of the film. Water analysis, using ion chromatography (IC), and ion-coupled plasma atomic emission spectra (ICP-AES), determined the chemical environment of the films. Future work is suggested related to film formation, composition and associated environmental conditions.

BACKGROUND

There are two states of iron, reduced and oxidized. The oxidized, or ferric, state (Fe^{3+}) is soluble in the very low or very high pH ranges and therefore precipitates in the circumneutral region (Cornell and Schwertmann, 2003). Iron transport through groundwater and soils occurs dominantly in the more soluble reduced, or ferrous, state (Fe^{2+}). Cornell and Schwertmann (2003) include iron oxides, iron hydroxides, and oxi-hydroxides in their definition of iron oxides, which will be used in this thesis. Iron in most minerals that make up the iron oxides is ferric, but some ferrous forms, such as $Fe(OH)_2$ occur. Some oxides include both ferric and ferrous iron, such as green rusts.

Visually, iron oxides often appear red-orange, or rusty. They may also be grey or blue-green in reducing conditions. In the laboratory, spectroscopy or diffractometry are common methods of characterization, as each oxide has distinctive characteristics that are discerned by these methods (Cornell and Schwertmann, 2003).

Cornell and Schwertmann (2003) identify sixteen iron oxides, including hematite, goethite, two-line and six-line ferrihydrite, lepidocrocite, magnetite, wüstite, $Fe(OH)_2$, and green rust. Oxides form under specfic conditions that include pH, temperature, redox characteristics of nearby water, and other minerals present. Goethite (α-FeOOH), hematite (α-Fe_2O_3), and ferrihydrite ($Fe_5HO_8 \cdot 4H_20$) are the most common iron oxides formed and are expected to form in environmental conditions similar to those in the coastal Oregon dune.

Iron Oxides in Surface Environments

Grathoff et al. (2003) identified ferrihydrite, hematite, and goethite in soil samples from the Oregon Coast. Ferrihydrite is the initial oxide to precipitate from reduced waters and over time it transforms into a more stable oxide such as goethite or hematite (Cornell and Schwertmann, 2003). This process is played out in the sand dunes along the Oregon Coast.

Iron on the Oregon Coast comes from the soil profiles of the weathered Pleistocene and Holocene dunes. Johnson (2003) suggested that iron is released as Fe^{2+} from weathering pyroxene in the B horizon, the origin of which is likely nearby volcanics. Fe^{2+} released from pyroxene weathering oxidizes into meta-stable ferrihydrite in soils or remains dissolved in the groundwater. In the soil profile soluble Fe^{2+} percolates downward to the C horizon where it oxidizes to goethite. Where the groundwater is discharged from the dunes the Fe^{2+} oxides as two-line ferrihydrite. The characteristic red-orange staining is observed where the iron has precipitated as an oxide.

Ferrihydrite is a poorly ordered iron oxide commonly divided into two crystal order extremes, two-line and six-line (Cornell and Schwertmann, 2003). The two crystal forms are based on the number of diffraction lines found in XRD patterns. Cornell and Schwertmann (2003) describe the shift from six-line to two-line as a decrease in crystallinity due to the faster rate of Fe^{3+} hydrolysis or as the Fe^{2+} oxidation is hindered by the presence of silicate or soil organic matter. Once formed, six-line ferrihydrite does not change to two-line, and vice versa.

Ferrihydrite can form biotically or abiotically. Abiotically, ferrihydrite forms directly from rapidly hydrolysed Fe^{3+} iron solutions or as a result of oxidation of Fe^{2+} solutions. Overtime it changes into goethite; a more stable crystalline iron oxide (Cornell and Schwertmann, 2003). Biotically, bacteria precipitate iron in the form of ferrihydrite (Banfield and Zhang, 2001). The oxidation of iron provides these bacteria with energy. Johnson (2003) identified iron oxidizing–like organisms in the seep pools containing the films at Driftwood Creek.

Films and Biofilms

Microbiology plays an important role in natural systems. Some bacteria use sunlight as energy and are often the base of food chains. Other energy sources, besides sunlight, are available to bacteria, including metal ions that can be oxidized or reduced, depending on favorable conditions (Nagai et al., 2001). The presence of bacteria may be apparent in biofilms in the environment. Sheehan et al. (2005) define biofilms as a sticky coating formed by bacteria, as well as fungi, algae, protozoa, debris, and corrosion products that form on any moist surface. Biofilms may also be termed mats if they are thick, layered microbial communities.

Naturally occurring films may be described as forming biotically (Tazaki et al., 2002 and Nagai et al., 2001) or abiotically (Schwertmann and Friedl, 1998). Abiotic formation includes oxidation into a precipitate. Biotically, films are created from bacteria that use nutrients in the water to create colonies, which often lead to mats, or biofilms. *Leptothrix* sp. and *Gallionella* sp. are two common iron oxidizing bacteria

species that live in circumneutral waters (Banfield and Navrotsky, 2001) similar to those found along the Oregon coast.

Iron-bearing films are not exclusively found in the coastal system. Schwertmann and Friedl (1998) described thin rusty films on the surface of pebbles submerged in ferriferous streams. The pebbles were of many different lithologies, so the origin of the film could not be linked to one type of rock. Mössbauer analysis of the films scraped off of several pebbles established the presence of goethite and ferrihydrite.

Tazaki et al. (2002) described the biomineral structures formed by *Leptothrix* sp. and *Gallionella* sp. biofilms. These iron biominerals include goethite, ferrihydrite, schwertmannite and amorphous iron hydroxides. The films formed within a few hours and changes in the films were observed for up to two months. The resulting films, made up of microorganisms and the adhered iron oxide were up to 10 nm thick. Ferrihydrite was identified as the initial mineralization product. Two months into the study the films were found to be composed of goethite.

Biofilms are particularly of interest to environmental geology because some bacteria, such as *Scenedesmus panonicus* and *Pseudomonas aeruginosa* remove heavy metals such as arsenic, chromium, and lead from contaminated water systems (Nagai et al. 2001). In a study by Nagai et al. (2001) the effects of arsenic and iron precipitating bacteria were observed in biomats about 10 cm thick. They found bacillus type bacteria about 1.0 µm in size as well as hydrous iron oxides. With the iron or heavy mineral trapped in the cell wall of the bacteria it will not travel further in

solution and contaminate other sources. The biofilms or the sediment containing the bacteria may then be removed or capped to protect from future contamination by the heavy metals.

Konhauser and Ferris (1997) identified films formed by iron-oxidizing bacteria in tropical rivers in Brazil and temperate rivers in Ontario, Canada as well as metal contaminated lake sediments in Ontario. In a study involving groundwater treatment systems Tinholt and Wendling (1997) indicate that the environment of groundwater treatment systems in British Columbia, Canada, promotes oxidation of dissolved iron and the growth of iron oxidizing bacteria due to the elevated dissolved iron levels present.

This study examined the possible role bacteria might play in the formation of the films. To incorporate both biotic or abiotic formation the films discussed in this study were termed iron-bearing films. Specific biotic or abiotic processes of iron-bearing film formation are identified as such where needed.

Geologic Setting

Sand dune sheets between 1 and 6 km wide and 30 to 100 km long (Cooper, 1959; Peterson et al., 2005) are extensive along the west coast (Figure 1). Peterson et al. (2005) determined that the dune deposits were emplaced during the Pleistocene and Holocene epochs. The Pleistocene dunes likely migrated onshore from continental shelf sand that was exposed to eolian processes during lower sea-level stands. The Holocene dunes are derived from beach sand transported shoreward during the last

transgression (Peterson et al., 2005). Weathering by soil and groundwater has redistributed iron, aluminum, and silica within the dunes (Grathoff et al., 2001).

This study will focus on Pleistocene dunes near Seal Rock State Park (UTM 10 413820 E 4927870 N) and the Driftwood Creek Wayside area (UTM 10 413820 E 4924430 N) in the Newport Dune sheet (Figure 2). The Driftwood Creek Wayside and Seal Rock sea cliffs are underlain by wave-cut platforms carved into late Pleistocene marine terrace deposits or Tertiary sedimentary rocks (Hart and Peterson, 1997).

The Pleistocene dunes contain a number of loess-enriched paleosols, which appear to control the groundwater flow and hydrochemistry of the area (Peterson et al., 2005). The paleosols and various cemented dune strata also affect the cut slope stability of the dunes with their low permeability ($10^{-5} – 10^{-7}$ K) (Clough, 2005). Slope stability is further affected by the cements holding the grains together. The cements include gibbsite, allophane, ferrihydrite, goethite, and hematite (Johnson, 2003).

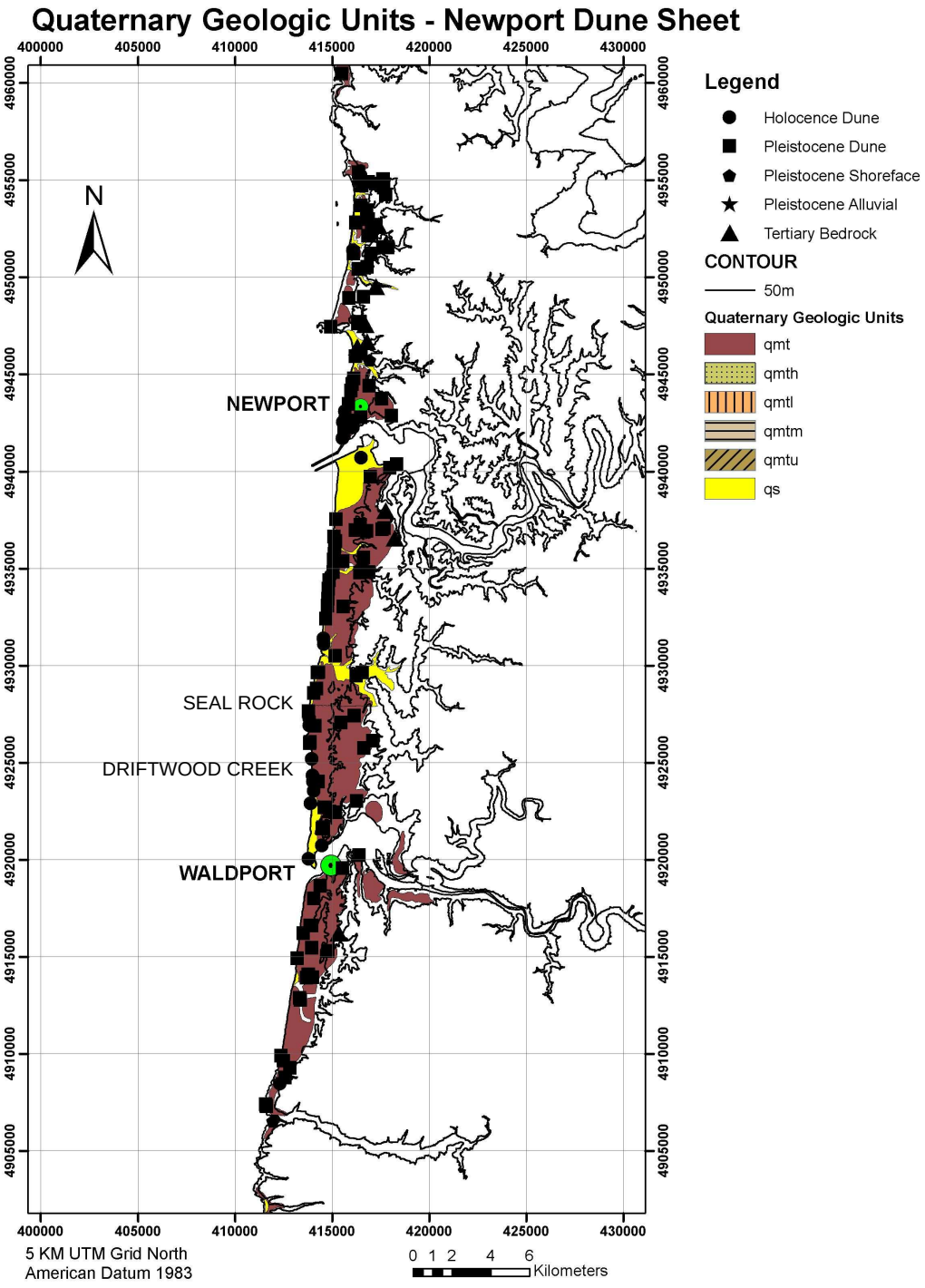

Figure 2. Geology of the Newport Dune Sheet. Samples were collected from Seal Rock and Driftwood Creek (Peterson, et al., 2005).

Well logs inland of Seal Rock and the area above Driftwood Creek State Park, in proximity to the study sites indicate that the local geology is predominantly sandy material, with evidence of interbedded gravel and clay (Oregon Water Resources Department, 2005). Aquifers at both locations are unconfined. Groundwater levels inland of Seal Rock range between 2.4 and 16.8 m below ground surface. At the Seal Rock site the groundwater is observed to seep out onto the beach where the permeable Pleistocene dunes overlie the less permeable Yaquina Formation (Figure 3). Inland of the Driftwood Creek site the groundwater levels vary from 2.1 m to as deep as 27.4 m below ground surface. At the Driftwood creek site the groundwater discharges in the form of seeps and springs where the Pleistocene sand dune deposits are in contact with groundwater saturated beach sand at the foot of the sea cliff (Figure 4). Water-well logs were obtained from the Oregon Well Water Program, which supplies well logs online (Oregon Water Resources Department, 2005). On the central Oregon coast rainfall averages between 39.9 cm from April to September to 136.8 cm from October through March (Taylor, 2005). Temperatures average 16.2 °C from April to September and 13.5 °C from October through March (Taylor, 2005).

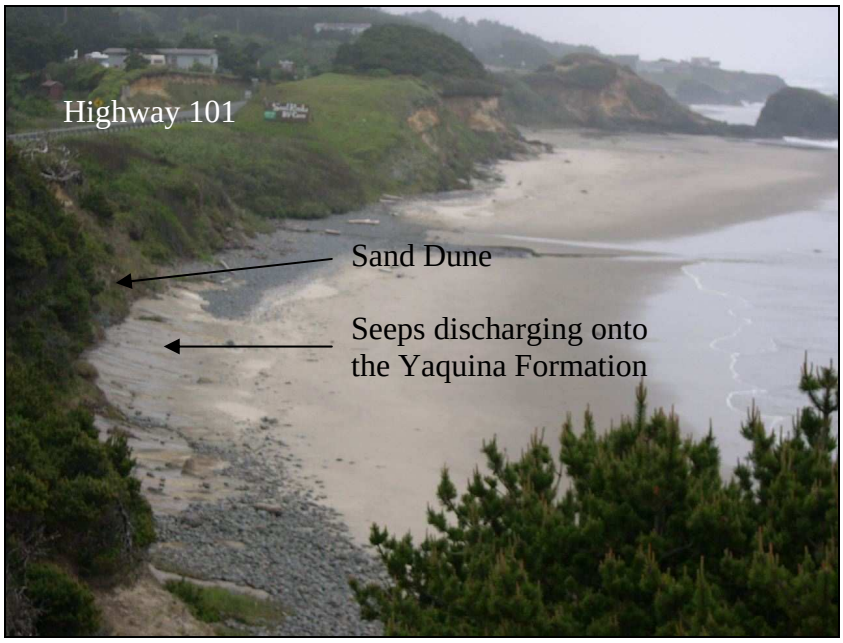

Figure 3. View of Seal Rock beach. Water is seen seeping out of the contact between the sand dunes and the Yaquina Formation below the trees on the left.

Figure 4. View of Driftwood Creek Wayside north of entrance to the beach. Water is seen seeping out of the base of the sand dune onto the beach.

Many coastal aquifers have high concentrations of dissolved iron and other nutrients, such as nitrogen and phosphorus (Thomas, 1995; Campbell and Bate, 1998). Reducing and oxidizing conditions influence the total iron concentrations detected in the groundwater. In dunal aquifers along the Oregon coast the water rises and falls seasonally, exacerbating the complexity of iron reduction and oxidation at different subsurface depths. This includes iron cements (Grathoff et al., 2003) and iron-bearing films on seeps below the dunes.

Groundwater conditions throughout the Oregon coastal dunes are similar. The average concentration of total soluble iron in the Coos Bay dune aquifer is 2.5 ppm with a pH range of 6.4 to 8.4 (Brown and Newcomb, 1963). In the Clatsop Beach Plains the pH ranges from 6.2 to 8.0, with iron concentrations mostly between 1 to 10 ppm. The highest iron concentrations from wells in the Clatsop aquifer reached 53 ppm (Frank, 1970). The EPA standard for iron in domestic and public water is 0.3 ppm. Where groundwater is removed for human use such high levels of iron may be problematic. Reducing conditions in an aquifer increase the dissolved iron, leading to diminished drinking water quality (Frank, 1970). Excessive iron in well water can form iron precipitates in pipes, filters, and appliances (Cornell and Schwertmann, 2003).

In Washington, similar groundwater conditions are also found. Iron in the Long Beach Peninsula in Washington ranges from 0.004 to 37 ppm, where the higher concentrations of iron, as well as nitrogen and phosphorus, corresponded to overlaying soils that were rich in organic matter (Thomas, 1995). Objectionable levels of iron,

relating to drinking water standards, were found by Slaughter (1962) in Pleistocene dune aquifers in Delaware and Maryland.

In waters with a pH of 6 or less and an Eh of less than 200 mV Fe^{2+} is the dominant form of soluble iron. Fe^{3+} dominates in waters with Eh values greater than 200 mV. Goethite and ferrihydrite start to form when the pH and Eh increase (Skinner and Fitzpatrick, 1992). Detailed groundwater analyses have been performed for the seeps and dune aquifer sources discussed in this study. Those analyses are in preparation by John Baham and Nick Chambers, in the Soil Sciences Department of Oregon State University, Corvallis, Oregon.

SITE DESCRIPTION

Driftwood Creek Wayside

Driftwood Creek Wayside is located at UTM 10 413820 E 4924430 N, at a distance of 28.8 km south of Newport, Oregon. The parking lot is on the west side of Highway 101 with an entrance to the beach to the north. Continuing north on the beach for several hundred meters, across Fox Creek, the seeps are visible. Iron staining is common, as well as iron-bearing films. Samples were collected in the seeps just north of Fox Creek and several hundred meters further north of the creek where they exit the Pleistocene dune sea cliff. These sites are located directly west of Orcas Road.

Driftwood Creek Wayside contains a Holocene dune cap overlying Pleistocene deposits (Figure 5). Houses have been built at the top of the dunes with vegetation growing down the dune slope (Figure 4). Water flows out from these dunes and seeps onto the beach, observed flows may be as high as several liters per minute. The pH of the water ranges from 5.4 and 6.7, with higher iron concentrations corresponding with higher pH. Where seep pools are present, iron may be observed in several forms: as red-orange staining on the sand, as orange-brown flocculent in slowly flowing pools, or as iridescent iron-bearing films formed on the surface of non-flowing water. No iron was visually apparent in the more rapidly discharging seeps. During the summer the films occur about 100 m from the ocean. During the winter the beach erodes and low tides may be 50 m away. High tides during the winter occasionally wash over the seeps.

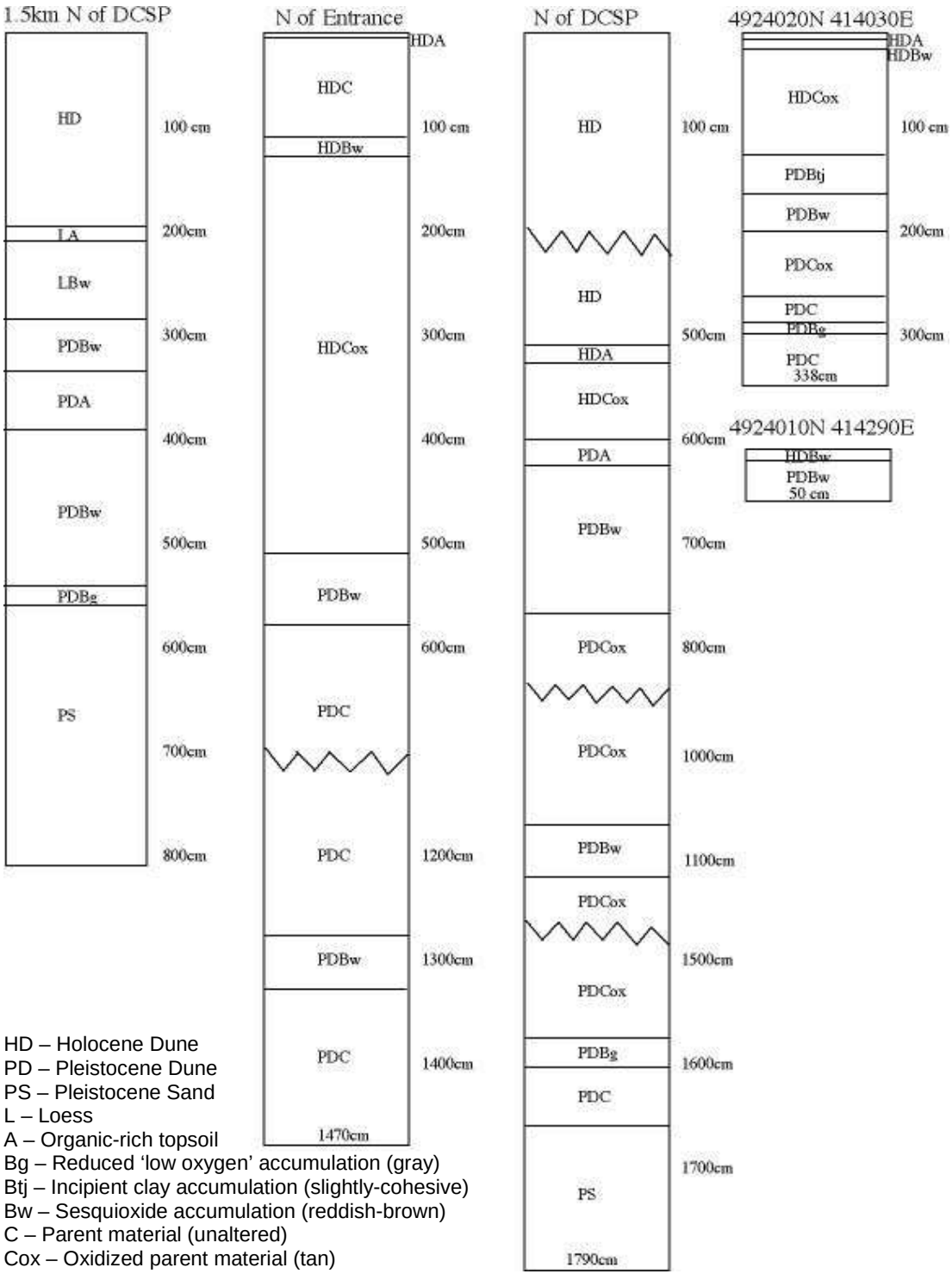

Figure 5. Stratigraphic columns of area surrounding Driftwood Creek State Park (DCSP) (Clough, 2005). Most of the seep pool sampling and a shallow monitoring well (Orcas) are located approximately at the left-most column, 1.5 km north of the entrance to the beach.

Seal Rock

Seal Rock is located at UTM 10 413820 E 4927870 N, a distance of 25.6 km from Newport, Oregon. The parking lot is on the west side of Highway. 101. Trails down to the beach are located to the southwest of the parking lot. Seeps may be seen along the Pleistocene dune sea cliff that makes up the east side of the beach several hundred meters to the south. Samples were collected from these seeps and iron-bearing films were seen at the more southern seeps.

Pleistocene dune deposits at Seal Rock State Park overlie a Miocene basalt sill that has intruded into the westerly dipping Yaquina Formation (Gamer, 1974) (Figure 6). Highway 101 runs directly behind the park. Groundwater exits the sea cliff at the base of the dune deposits, which are in contact with the bedrock wave-cut platform (Figure 7). While the base of the dunes is generally damp, several outlet streams are present. Films are found in the pools and side channels of these outlets. No seeps were observed to exit the dunes at this location with a flow greater than 1 L/min. The films at this location occur about 20 m from the ocean during summer and low winter tides. High winter tides may come up to the seeps. Seal Rock gets its name from a basalt dike located just offshore. This feature creates larger waves and more sea spray than at Driftwood Creek.

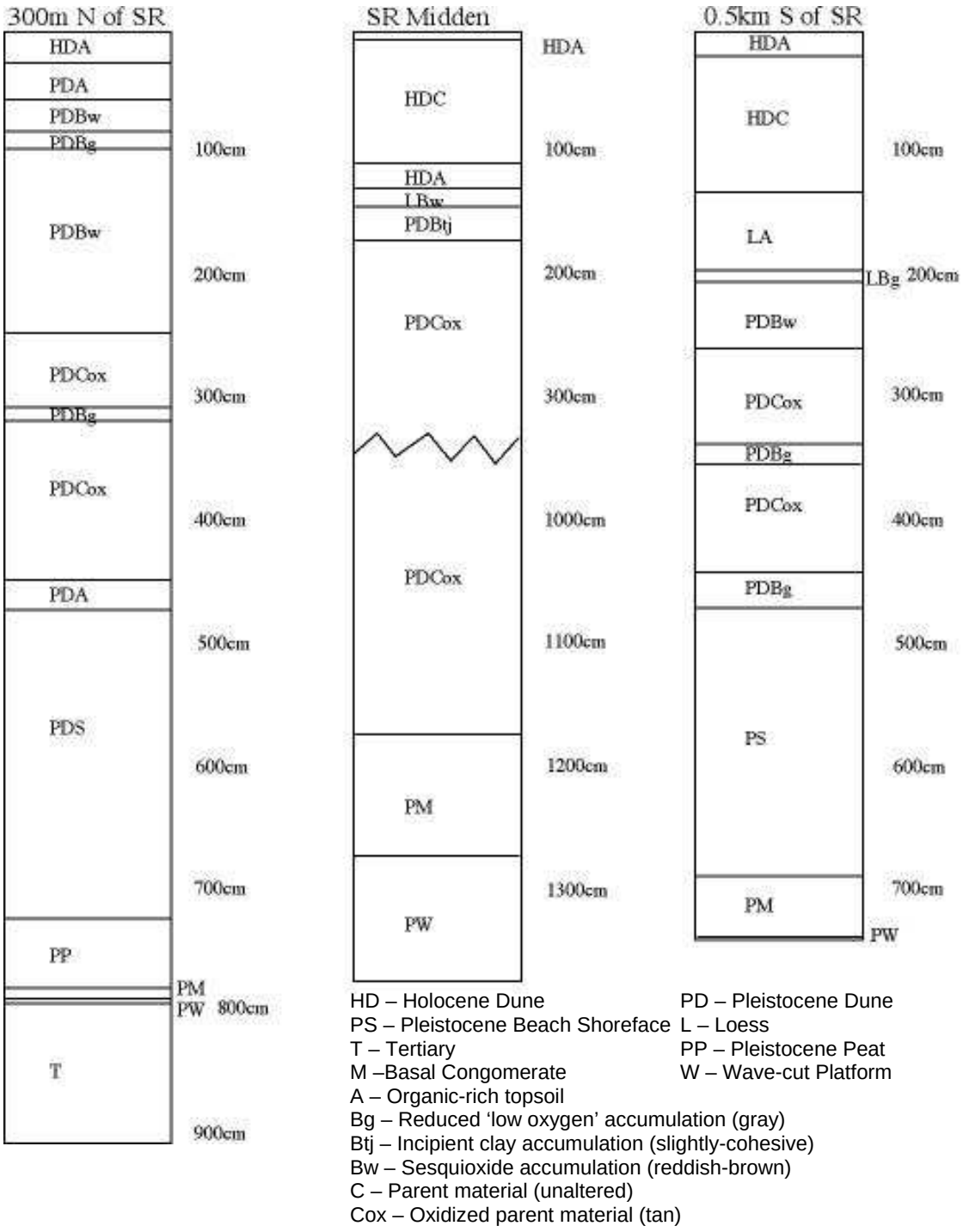

Figure 6. Stratigraphic column of the area surrounding Seal Rock State Park (Clough, 2005).

Figure 7. The point of the arrow is on the wave cut platform where seeps appear at Seal Rock State Park. Samples were collected at the seep directly east of the end of the arrow.

The amount of visible iron present at Seal Rock is less than at Driftwood Creek. There is little orange-brown flocculent to be found in the seep streamlets, although the discharge area is of similar length to that of Driftwood Creek and red-orange staining is present in places. Some small biomasses may be seen in small pools where films are not found, these are green-brown and stringy in appearance, more like algae than the flocculent associated with the iron-bearing films.

FIELD METHODS

Film samples from the surface seeps were collected on various types of substrates, including glass slides, ZnSe slides, plastic slides and carbon stubs. Flocculent from the bottom of the pools was also collected. Sample sites and conditions were logged in a notebook. Water samples were collected at Driftwood Creek. Due to the low water discharge at Seal Rock, water samples were not collected from that site.

Samples were collected similarly, despite collection on different substrates and for different analytical methods. Substrates included carbon stubs, or a glass, ZnSe or plastic slides. Iron-bearing films were collected by placing a substrate on the surface of a film-coated pool, the film would adhere onto the substrate with little disturbance to its form. To prevent further oxidation glass slides were placed in a centrifuge tube and capped. However, if left in the open air the film would slowly turn from a clear iridescent to the reddish-brown commonly seen in oxidized iron. The ZnSe slides were put into argon atmosphere tubes created out of PVC pipe for Fourier transfer infrared (FTIR) analysis (Figure 8). This insured the least amount of oxidation and disturbance to the film for this sensitive analysis. For scanning election microscope (SEM) analysis the carbon stubs were dipped in the film and put in an open-air traveling container for transport back to the laboratory (Figure 9).

Figure 8. Sample holder for FTIR samples. Argon is pumped through the tube on the right and the sample is inserted by unscrewing the left end.

Figure 9. Carbon stubs with film in the transport container.

Film collection on TEM grids varied slightly between samples. Using an eyelash probe (Figure 10) in the seep pool a small amount of film was gently guided

toward the grid. The grid, held by tweezers, was first cleaned with acetone and allowed to dry. The grid was then placed in the water next to the desired film sample and the eyelash probe was used to push the film toward the grid, which was at the same time moving toward the film. Once the film was over the grid both were removed from the water. Filter paper was used to wick the excess water off the backside of the grid. The grid was then air dried for 5 to 10 minutes to remove any water trapped between the tweezer's blades. Finally, the grid was then returned to the open-air box for transport back to the laboratory.

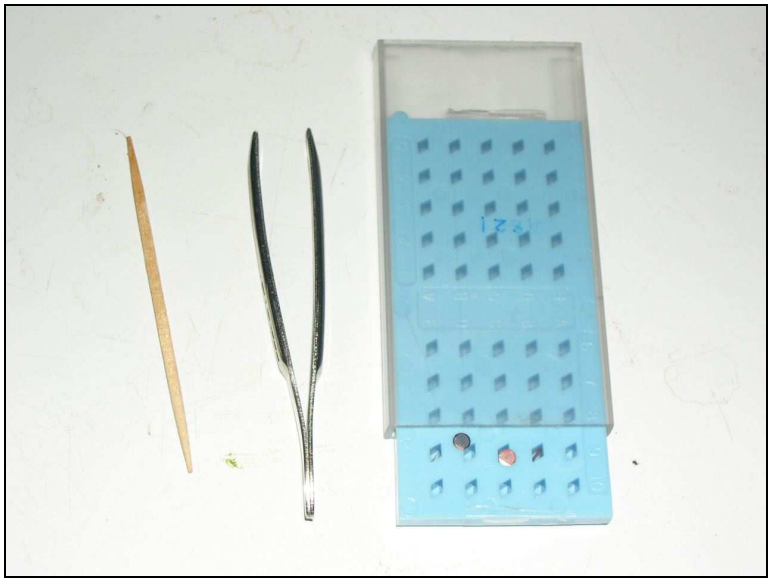

Figure 10. Tools for TEM collection (from left to right) eyelash probe, tweezers, TEM copper grids.

Water samples at Drift Creek were collected for anion and cation analysis. A portable probe was used to determine the *in situ* pH, as well as conductivity, water temperature, redox values, and the total dissolved solids (TDS). Water was collected with a 0.45 µm pore size Whatman Syringe Filters. Additonally, cation sample bottles

had been acidified with 5 mL of NO_3 to 120 or 180 mL of sample water collected in the field. Estimates of the dissolved Fe^{2+} and oxygen were taken during some sampling trips using CHEMets Tests.

LABORATORY METHODS

X-ray Diffraction

Mineral identification was performed using a Theta-Theta Philips PW3040 X-Ray Diffractometer with an Energy Dispersive Peltier Cooled Kevex detector. Operating conditions were at 40 kV and 30 mA with step sizes between 0.02 and 0.025 °2θ, count times of 0.6 seconds were used for continuous scans while 1, 3 or 25 second count times were used for step scans. All scans were run from 3 or 5°2θ to 75 or 100°2θ. The film was analyzed on quartz zero background (QZB) slides, which was then compared to the substrate without the film. Samples were analyzed with both a Cu and a Co tube.

XRD analysis also included powder of the scraped iron-bearing films on a quartz zero background slide. The film was scraped off the initial collection glass slide with a razorblade and analyzed on the zero background sample holder by top packing the film into a 0.2 mm deep cavity with a diameter of 10 mm. Random powder analysis was also performed on the flocculent (Moore and Renyolds, 1997).

Scanning Electron Microscopy

Three sample collection and mounting protocols were used to prepare the samples for analysis by scanning electron microscope (SEM). The first method involved a piece of glass cover slip that was coated with film and adhered to a carbon or aluminum stub using carbon tape. The second method involved transferring the iron-bearing film directly onto the carbon stub in the field. In the third method, the

films were transferred in the field onto plastic cut from a clean piece of plastic and then adhered to the aluminum stub with carbon tape.

The glass slide contained too much silica to constrain the major constituents while the carbon stub was contaminated with iron during coating from the sample holder, again hindering the proportions of major constituents of the film. The plastic slide was thought to be a good compromise, but it also contains silica. Blank slides were analyzed for comparison to sample loaded slides to establish background compositions.

All film samples were coated with carbon using a Gatan Precession Etching Coating System Model 682. Samples were analyzed using a Joel 35C Scanning Electron Microscope at 15 kV accelerating voltage. The machine was equipped with a Kevex X-ray detector for use in Energy Dispersive X-Ray Spectroscopy (EDS). Samples collected on the plastic slides were used for quantitative EDS analysis to determine relative amounts of silica and iron with a dead time of 30%. The film was tilted to 45° in preparation for EDS analysis and for a better look at the sample film thickness.

One sample collected on a glass cover slip was coated with gold-palladium in preparation for high resolution SEM (HRSEM) EDS. The sample was analyzed on a FEI Sirion Field Emission Scanning Electron Microscope equipped with an Oxford Inca Energy 250 EDS system at 5 kV.

High Resolution Transmission Electron Microscopy

Films were colleted on carbon coated 300 mesh copper TEM grids with an eyelash probe. Samples were coated with a thin layer of carbon in a Gatan Precession Etching Coasting System Model 682. Samples were analyzed using a FEI Tecnai G2F20 HRTEM with a voltage of 200 keV for crystallographic analysis. Parallel Electron Energy Loss (PEELs) analysis was used on several locations on the film to determine the different compositions of the film. Dr. Rick Hugo of Portland State University performed the analysis.

Thermogravimetric Analysis

The powder from XRD analysis was loaded into a Perkin Elmer TGA7 Thermogravimetric Analyzer (TGA). A sample of 3 mg was heated from 50º C to 950º C with a heating rate of 10º C/min. The sample almost filled the analysis dish. The resulting weight percent loss was compared to the temperature to reinforce conclusions on the chemical makeup of the films.

Optical Microscopy

The morphology of the films, the water, and the seep bottom flocculent were examined using a Leica DMRX microscope with a Apogee KX2D Camera. Phase imagery was used on all samples to view the film and water, as well as to compare morphology to the images collected under dark-field. Bacteria are not easily seen under phase conditions without staining. Therefore dark-field imagery was used in

visual characterization of the bacteria present. All methods mentioned thus far were analyzed at Portland State University.

Ion Chromatography

Anions were analyzed at Portland State University using a Dionex 2500 Ion Chromatography (IC) system with autosampler consisting of a GP50 gradient pump with an IonPac AS-14A column, a LC25 chromatography oven, and CD25 conductivity detector. Carbonate eluent with election suppression with a 1mL/min flow rate was used. Samples were analyzed for total soluble F^-, Cl^-, NO_3^-, PO_4^{3-}, and SO_4^{2-}. Analysis of additional samples, collected in early 2005, were performed by Nick Chambers, Soil Science Department, Oregon State University.

Inductively Coupled Plasma-Atomic Emission Spectrometry

Total dissolved aluminum, calcium, iron, magnesium, potassium, silicon, and sodium were measured for the water samples on a Varian Liberty 150 Inductively Coupled Plasma-Atomic Emission Spectrometer (ICP-AES) run with a V-groove nebulizer and a Varian SPS5 autosampler system. Table 1 shows the wavelengths under which the samples were analyzed. Samples were analyzed by Nick Chambers of the Soil Science Department of Oregon State University.

Table 1. Wavelength parameters for AES analysis.

	Al	Ca	Fe	Mg	K	Si	Na
Wavelength (nm)	394.4	422.7	259.9	280.3	766.5	251.6	589.6

Colorimetric Determination of Ferrous and Ferric Iron

Samples of the film were collected on Pall Gelman glass fiber filters. Each filter was wiped across the film about four times to cover the filter paper completely. The glass filters were then placed in a glass vial filled with 22 mL of 0.1M HCl. Sample blanks were collected by placing filters from the package that had not been dipped in film into the sample bottles.

Samples were stored in the dark until analyses were preformed. The concentration of Fe(II) in the acid solution was measured colorimetrically using a variation of the 1, 10-phenanthroline method (Loeppert and Inskeep, 1996) at 510 nm. After reducing all of the soluble iron to Fe^{2+} with hydroxylamine hydrochloride samples were measured again to determine the total iron. The difference between the total iron and the ferrous iron gave the amount of ferric iron. All reactions were conducted in an 8 mL ramin electronic pipette test tube to insure the same concentrations. Analysis was done at Oregon State University by John Baham and Nick Chambers of the Soil Science department.

Fourier Transfer Infrared Spectroscopy

Infrared spectra from the films were collected using a Bruker IFS66/S Fourier Transform Infrared Spectrometer (FTIR) utilizing a Michelson interferometer and equipped with an infrared microscope. The spectrometer and microscope were purged with nitrogen gas to diminish strong absorbencies due to atmospheric carbon dioxide

and water vapor. Spectra were collected at 4 cm^{-1} spectral resolution over the frequency range of 4600 to 400 cm^{-1}, using a DTGS detector, a KBr beamsplitter, a mid-infrared Globar source. Spectra were obtained from 128 co-added scans acquired from double-sided/forward-backward mirror motion and with a mirror velocity of 10 kHz. Spectra were acquired while using a 16 kHz low pass filter to prevent aliasing, using a zero filling factor of 2 and Norton Beer medium apodization, and 16 cm^{-1} phase resolution and Mertz phase correction.

Spectra were collected using conventional transmission measurements of the ZnSe supported film in the sample compartment of the bench. Spectra were also collected in transmission and reflectance modes using the infrared microscope, also with the film on the window. A fourth set of spectra were collected using a grazing angle (85°) specular reflectance accessory.

Samples were analyzed by FTIR on ZnSe slides at Pacific Norwthest National Laboratories in Richland, Washington by Dr. Paul Gassman. Samples were analyzed under the conditions in which they were received.

RESULTS

Iron-bearing film samples were collected from Seal Rock and Driftwood Creek between 1/20/04 and 3/21/05 (Table 2). At Seal Rock film samples were taken from the only seep that typically produced film. There was not enough water discharged to collect water samples. Samples from Driftwood Creek include both film and water samples. Sampling environments at Driftwood Creek included one seep pool that remained full, a small stream mouth that disappeared after winter storms reworked the beach, and several seeps that could be found for about a month at a time before they dried up or moved. A shallow groundwater well at Driftwood Creek, installed for a parallel study, was used to compare groundwater to surface water conditions. The pH at Driftwood Creek ranged between 4.8 and 6.7 in the seeps and 5.4 and 5.8 in the well.

Analytical results for Driftwood Creek include XRD, SEM, FTIR, optical microscopy, IC, and ICP-AES. Due to the lower concentration of films at Seal Rock only XRD and SEM analyses were performed. Types of sampling and the dates they were collected are shown in Table 2.

Table 2. Dates that field sampling took place and the samples that were collected from both Driftwood Creek and Seal Rock.

Date	Sample Location	Sample Type Collected						
		Glass Slide	QZB Slide	FTIR	Water	SEM	TEM	Flocculent
1/20/04	Driftwood	X						
	Seal Rock							
5/8/04	Driftwood	X			X			
	Seal Rock							
7/31/04	Driftwood	X				X		X
	Seal Rock	X						
8/31/04	Driftwood					X		
	Seal Rock					X		
9/25/04	Driftwood	X			X			
	Seal Rock	X						
10/13/04	Driftwood	X			X			
	Seal Rock							
11/10/04	Driftwood	X	X		X			
	Seal Rock	X	X					
11/17/04	Driftwood	X		X	X			
	Seal Rock							
1/8/05	Driftwood				X			X
	Seal Rock							
2/5/05	Driftwood			X	X		X	
	Seal Rock							
3/21/05	Driftwood	X						
	Seal Rock							

Field Observations

The films appear in the quiescent areas near seeps and streams discharging from the sand dunes (Figure 11). The film appears to be oily and iridescent on the surface of the seeps (Figure 12). When conditions are calm layers of film build up, changing the appearance from translucent to more opaque. In Figure 13, taken on September 25, 2004, after approximately a week without rain, both the thick and thin layers of the film may be seen. Disturbances break the film up into small platelets

(Figure 14). Bugs and dust have been observed to sit on the film without disturbing it, indicating that the surface tension is at least as high as that of water. The film often starts growing around plants, as the stalks often help slow the water enough for the film to form.

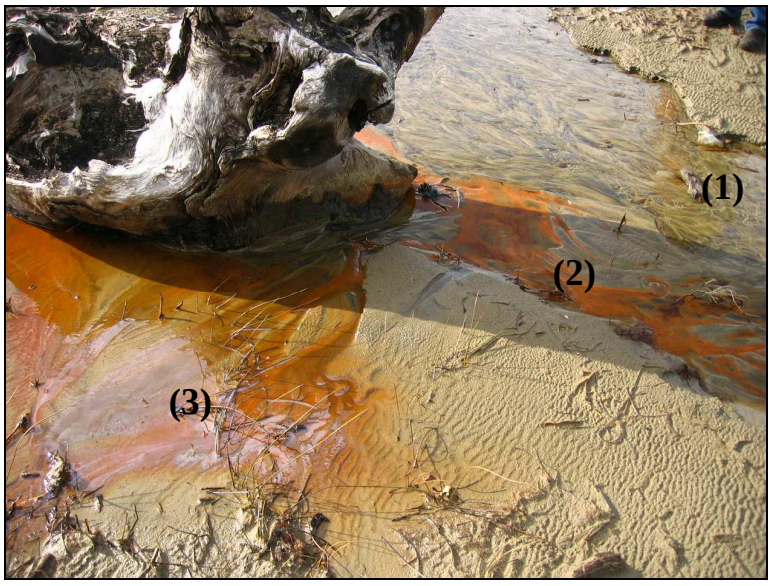

Figure 11. Seep area of Driftwood Creek that shows the three environments (1) the flowing water, (2) the red-orange flocculent, and (3) the irridescent iron-bearing film.

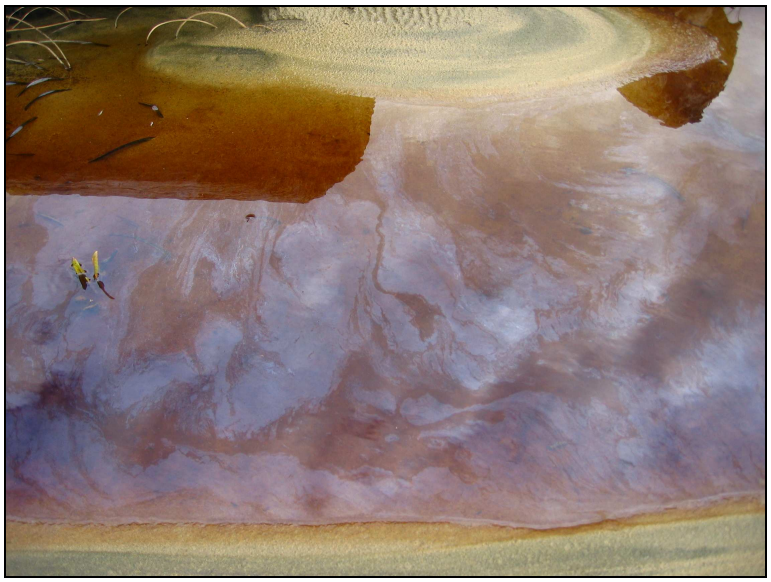

Figure 12. Oily appearance of the iron-bearing film at Driftwood Creek.

Figure 13. Layers of iron bearing film seen in September 2004 at Driftwood Creek after ideal conditions persisted for at least a week. The film, which may be seen growing around the plants, is thick in some areas and thin in others.

Figure 14. Iron-bearing film forming on the backwater of a seep at Driftwood Creek. The platy nature of the film is apparent in this picture.

Films naturally form rapidly, within a few minutes in the absence of strong winds and rain, which disturb the water surface enough that the film does not form. After a few minutes of calm conditions the film begins to reform. The formation rate of the films was tested by digging a hole in the sand down to the water table near a pool that contained film. Within 5 minutes film formation began in the test hole.

Optical Microscopy

For optical microscopy analysis three types of samples were collected 1) the film dried on a glass slide, 2) the film and some water from the surface of the pool and 3) the flocculent from the bottom of the pool (see Methods). All samples were examined to determine if any bacteria were present in the film or the near surface water.

The film on the glass slide was collected on QZB1 from November 10, 2004 from Driftwood Creek by dipping the slide onto the film and allowing the removed section to dry. Under the optical microscope, using phase conditions, the film was transparent light brown to iridescent in color, appearing very jagged and shard-like (Figure 15). The shards are lath or octahedral shaped and roughly 100 µm long.

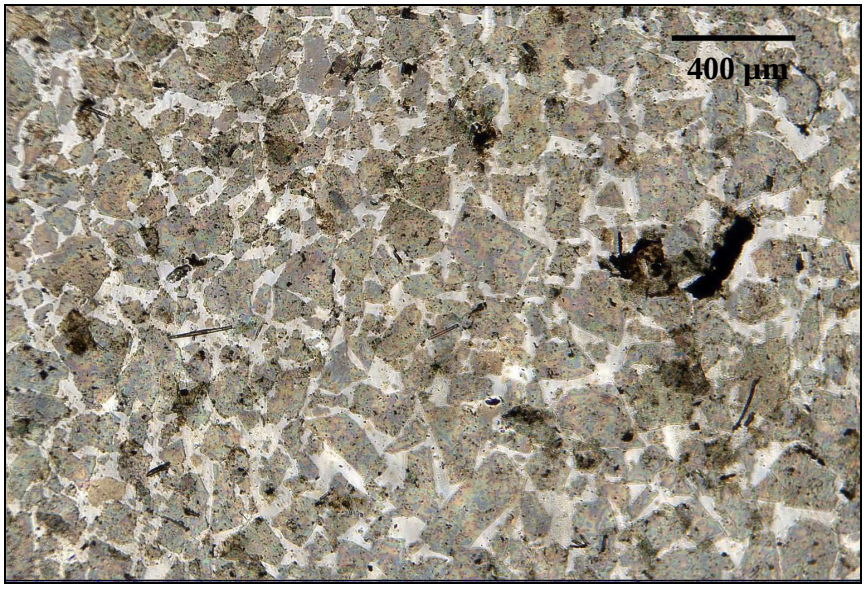

Figure 15. QZB1 at 10x under phase conditions. This is the dried film with its shard like brown-iridescent appearance. Parts of the film are orange-brown where the film appears be altering into flocculent.

Parts of the film are a brown-orange material, similar to the flocculent found at the bottom of the pools. This material is thick enough to be opaque in the concentrated centers and translucent on the wispy edges. It is most commonly found connected to the film. Figure 16 shows one location on QZB1, (A) is a dark-field

image while (B) is in phase lighting. This suggests that the film is the precursor to the flocculent. The film represents initial oxidation of the water surface, while subsequent oxidation/precipitation leads to the two-line ferrihydrite Johnson (2003) found on the bottom of the pool. No bacteria were found in the dried film.

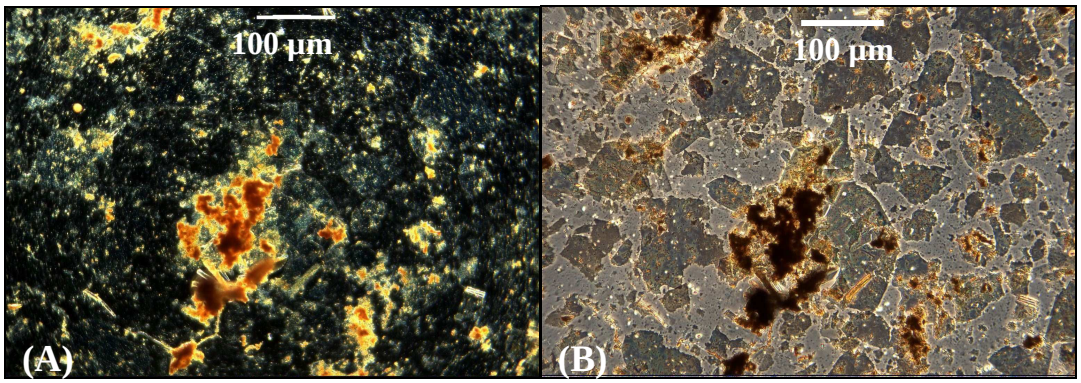

Figure 16. QZB1 at 20x. (A) is a dark-field image showing the flocculent as orange and with more depth than (B) a phase image of the same area showing the platy nature of the film and the brown appearance of the flocculent.

Water from the pools, collected with the film, did not contain suspended sediment (Figure 17). Upon precipitation to the flocculent phase, the ferrihydrite settles to the bottom of the pool. Diatoms and other single cell organisms were present in trace amounts, 2 organisms per 1 mL of water. No iron-oxidizing bacteria were found based on criteria for oxidizing bacteria morphology (Banfield and Zhang, 2001). Shards less than 300 µm wide, similar to those in the film found on QZB1, were also found. Some of the film had dried onto the side of the centrifuge tube used to transport samples from the field to the laboratory. These shards may have been cohesive enough to retrain their shape when pipetted onto the analysis slide.

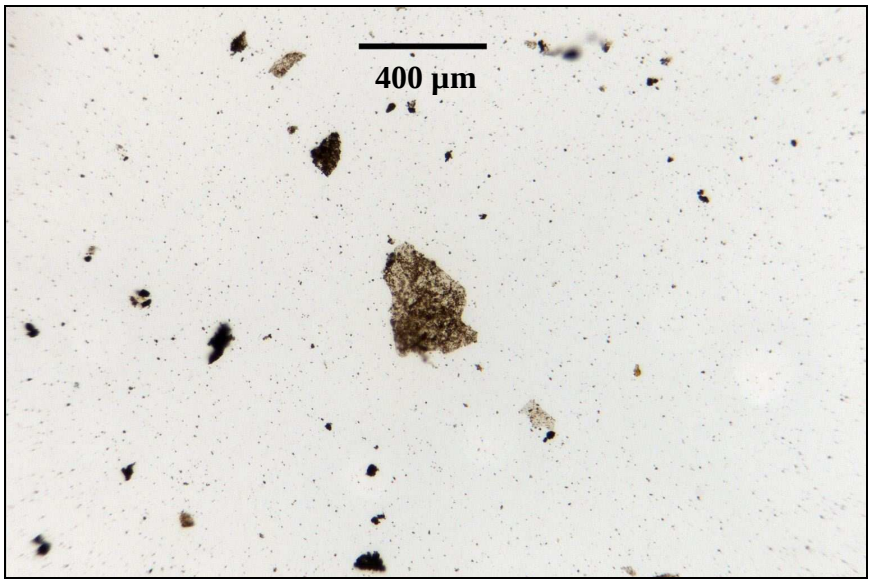

Figure 17. Driftwood Creek film and water at 10x. Among the diatoms and other single cell organisms found in the water is this shard-like material, about 100 by 200 µm, likely representing the film in a submersed state. No diatoms or other single cell organisms are seen in this micrograph.

The flocculent below the film showed many red-orange masses of oxide colored material, diatoms, and sheath-like bacteria about 5 µm by 150 µm (Figure 18). Sand grains were also coated with the flocculent. No shard like material was found mixed in with the flocculent. Dark-field imagery helped to discriminate the shard and/or flocculent morphologies, see the Methods Section for details.

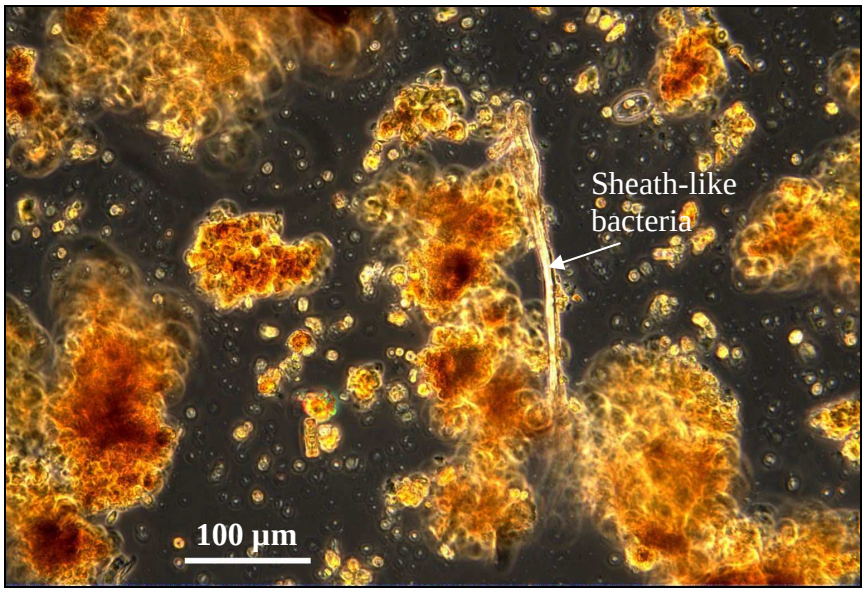

Figure 18. Flocculent at 20x. Dark-field image of the flocculent and bacteria from the bottom of a pool at Driftwood Creek. The bacterium is indicated with the arrow.

Scanning Electron Microscopy (SEM)

A total of nine samples of iron-bearing film were analyzed by SEM; including five samples on carbon stubs, four on plastic slides, and one on a glass cover slip for HRSEM. Samples are designated DC or SR for the two respective sites, Driftwood Creek and Seal Rock, with numbers corresponding to the number of total SEM samples collected from each site. Glass slides were not used in primary analysis due to the silica found in the film. The different substrates were used to detect differences in texture of the films and to constrain the amount of silica. Glass was only used for HRSEM where carbon could be detected.

Morphology between the two sites was similar under the SEM. Figure 19 shows a common appearance from the iron-bearing film. The film has low relief and shows cracks similar to those found in field observations. The plastic substrate is seen

through these cracks as a darker, flatter grey. Within the film are concentrated masses, seen in white under the SEM labeled flocculent in Figure 19. These white masses have high concentrations of iron, as determined in EDS. Similar to optical microscopy, the flocculent remains associated with the film as it ages.

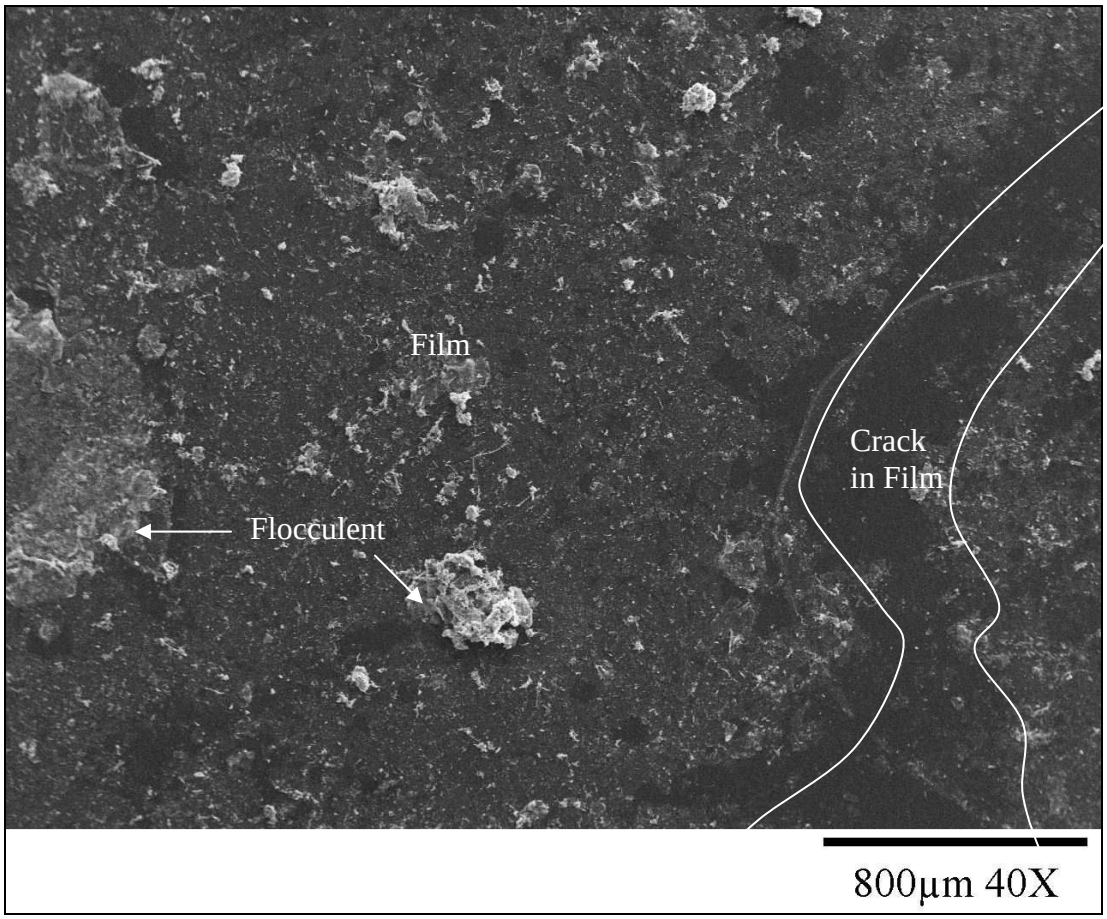

Figure 19. Micrograph of Seal Rock film (sample S3) on a plastic slide. The film is the medium grey material. A crack may be seen running through the film on the right of the picture, showing the darker grey substrate. To the left of the picture are white masses of flocculent.

At higher magnifications (of > 2000x) the platy nature of the film becomes better defined. A film thickness on the order of 100 nm may be observed in Figure 20.

The stringy nature of the flocculent and a potential sheath-like structure is also apparent in Figure 20. It is unclear if this is truly an iron-oxidizing bacterium or not (see later HRSEM micrographs of the sheath-like structures in the HRSEM section).

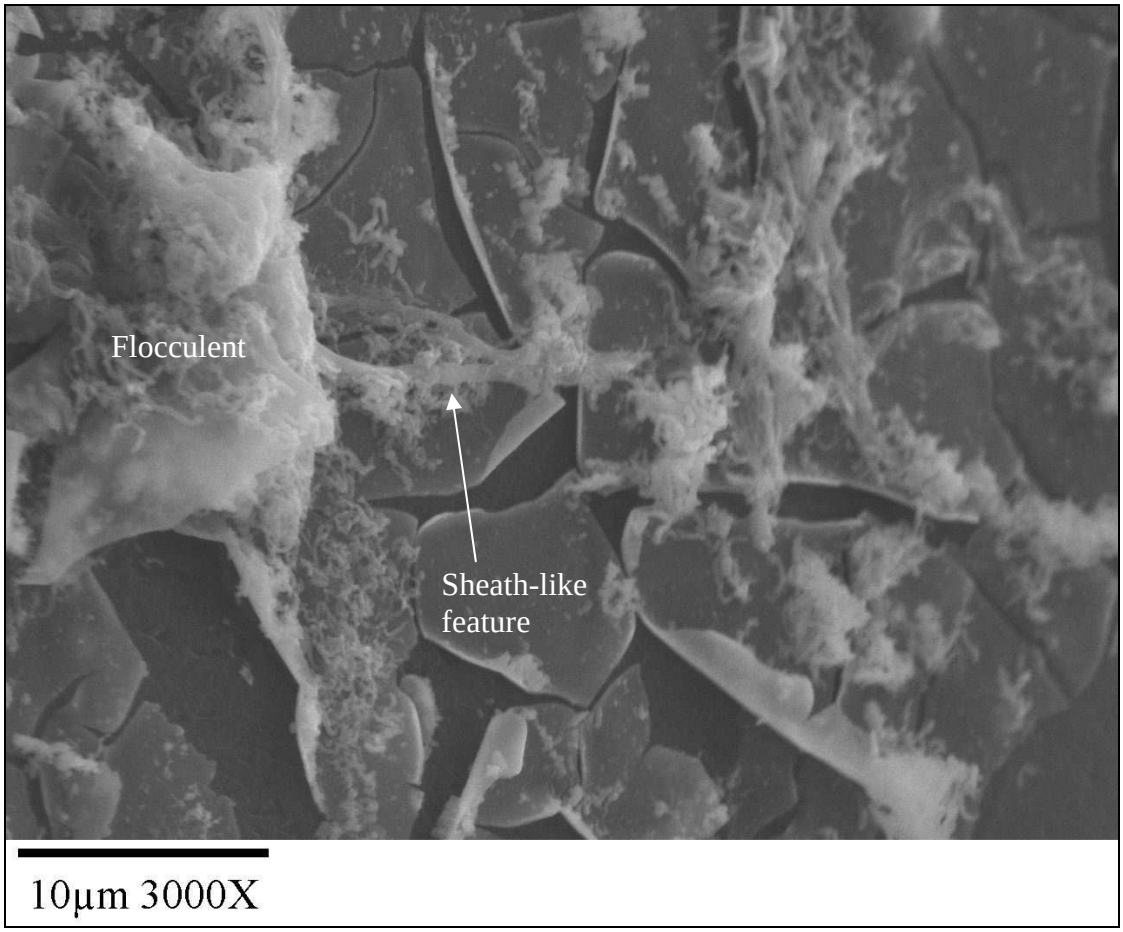

Figure 20. High magnification micrograph of sample D3 showing cracked morphology of the film and stringy morphology of the flocculent.

EDS quantitative elemental analysis showed that the film and flocculent are made of iron and silica. The iron to silcia atomic ratio is about 3:1. At Seal Rock, in addition to silica and iron, chlorine and sodium were also major constituents. However, no cubic halite crystals were found on the film and there is not substantial

sodium or chlorine in the substrates, indicating that these must be distributed throughout the film, likely on the surface due to sea spray. An example of an EDS spectrum is shown in Figure 21. Table 3 shows the atomic percent of the major elements in the film as determined by the quantitative EDS, including that of sample D4 Mar Film 2, shown in Figure 21. Locations of EDS spectra are in Appendix A.

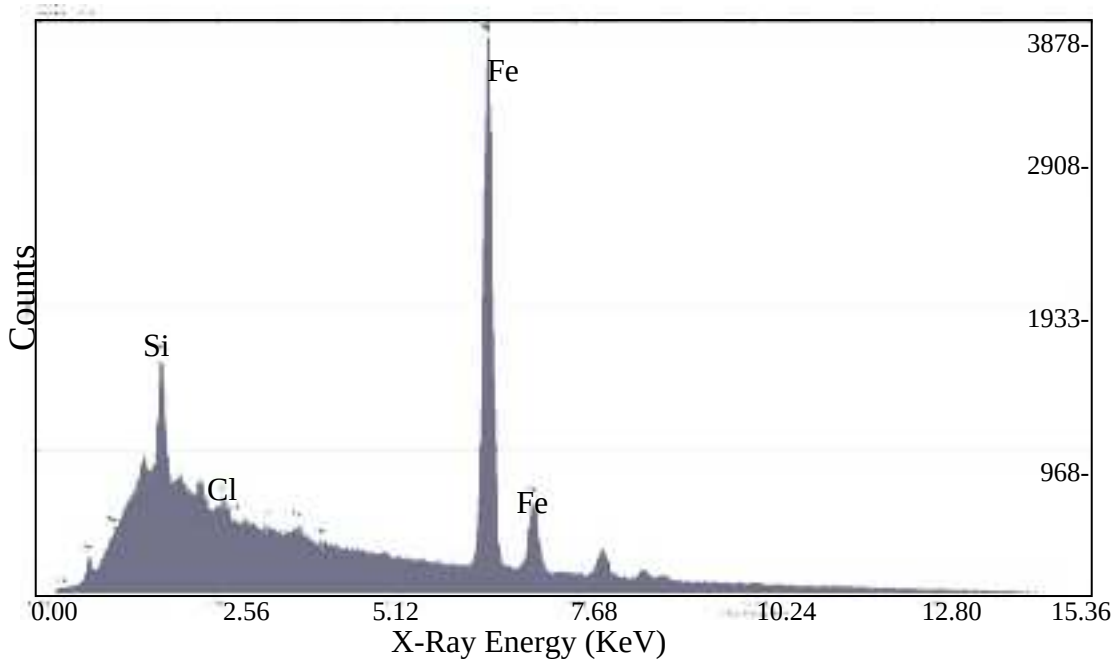

Figure 21. EDS spectra of sample D4 Mar Film 2 on the film with a dead time of 30%.

Table 3. Quantitative SEM EDX atomic percent of elemental constituents of samples. All samples are on plastic slides and blank plastic values are included below the sample values.

Sample Name	Element (at. %)						
	Fe	Si	Cl	Na	Mg	Al	Fe:Si Ratio
S3 Film 1	26.57	23.62	13.63	15.97	9.85	7.41	1.12
S3 Mar Film 2	37.39	24.67	13.28	9.29	4.93	4.60	1.52
S3 White 1	41.41	21.18	11.53	7.97	5.09	3.22	1.96
S3 Blank (hole)	27.77	18.63	11.17	14.59	7.21	5.42	1.49
S4 Film 1	39.27	26.57	5.66	10.05	8.30	7.89	1.48
S4 Mar Film 2	35.39	15.79	10.94	18.55	5.23	5.49	2.24
S4 White 1	42.61	28.05	7.33	8.84	6.14	5.63	1.52
S4 Mar White 2	66.86	22.6	0.73	2.52	2.62	1.30	2.96
S4 Blank (hole)	3.57	34.82	0.02	4.04	21.58	2.42	0.10
D3 Film 1	50	19.19	1.73	5.58	7.75	10.38	2.61
D3 Mar Film 2	49.7	18.68	1.55	3.75	8.42	13.43	2.66
D3 White 1	49.04	15.57	1.41	6.32	6.84	10.06	3.15
D3 Mar White 2	49.87	23.54	1.79	0.87	6.23	12.69	2.12
D3 Blank (hole)	35.69	23.21	1.31	7.33	4.18	15.37	1.54
D4 Film 1	50.74	18.25	1.71	3.92	5.21	9.75	2.78
D4 Mar Film 2	72.49	11.27	0.73	2.52	5.03	7.28	6.43
D4 White 1	57.23	13.5	2.17	4.02	5.18	8.20	4.24
D4 Mar White 2	61.92	14.68	0.49	4.29	7.58	10.29	4.22
D4 Blank (hole)	3.1	31.33	0.24	3.51	20.80	24.44	0.10
Blank Plastic 1	0.99	33.11	0.06	12.57	19.00	22.71	0.03
Blank Plastic 2	0.98	33.66	0.00	11.91	18.34	22.52	0.03
Blank Plastic 3	1.16	33.31	0.08	12.02	18.35	22.64	0.03
Blank Plastic 4	0.65	34.92	0.44	12.52	18.25	22.41	0.02

S3 and S4 are samples three and four, respectively, from Seal Rock
D3 and D4 are samples three and four, respectively, from Driftwood Creek
Film indicates location on the film
White indicates location on a white flocculent mass
Mar indicates samples analyzed in March at different sites within the slide

The background level of the silica in the blank plastic slides is high. These levels are not thought to corrupt the data due to cross analysis of carbon stubs. Carbon stubs were analyzed as well as the plastic slides. These stubs were contaminated with iron during coating, so their iron levels were unusable. The silica data were not influenced, and the levels are similar to what is seen in the samples on the plastic slides (Table 4). Table 3 and Table 4 should not be compared in anything other than silica levels due to the iron contamination.

Table 4. SEM-EDX atomic percent of elemental constituents of samples collected on carbon stubs.

Sample Name	Element (at. %)					
	Fe	Si	Cl	Na	Mg	Al
SR Carbon Film	28.18	23.01	12.45	7.88	6.89	10.29
SR Carbon White	34.16	30.92	11.94	10.14	2.06	2.97
DC Carbon Film	67.92	26.32	0.31	ND	2.43	2.89
DC Carbon White	56.04	25.35	0.46	ND	1.39	4.03

SR is a sample from Seal Rock
DC is a sample from Driftwood Creek
Film indicates location on the film
White indicates location on a while flocculent mass
ND = Not Determined

High Resolution Scanning Electron Microscopy (HRSEM)

One sample from Driftwood Creek was collected on a glass cover slip, coated with Au-Pd and analyzed in the high resolution scanning electron microscope. Under low magnification the film morphology was similar to that of lower resolution SEM (Figure 22). Similar cracks appear, as well as larger cracking features, which likely

came from water trapped under the film as it dried. The number of flocculent masses of comparable size to previous work were fewer, although they were visible.

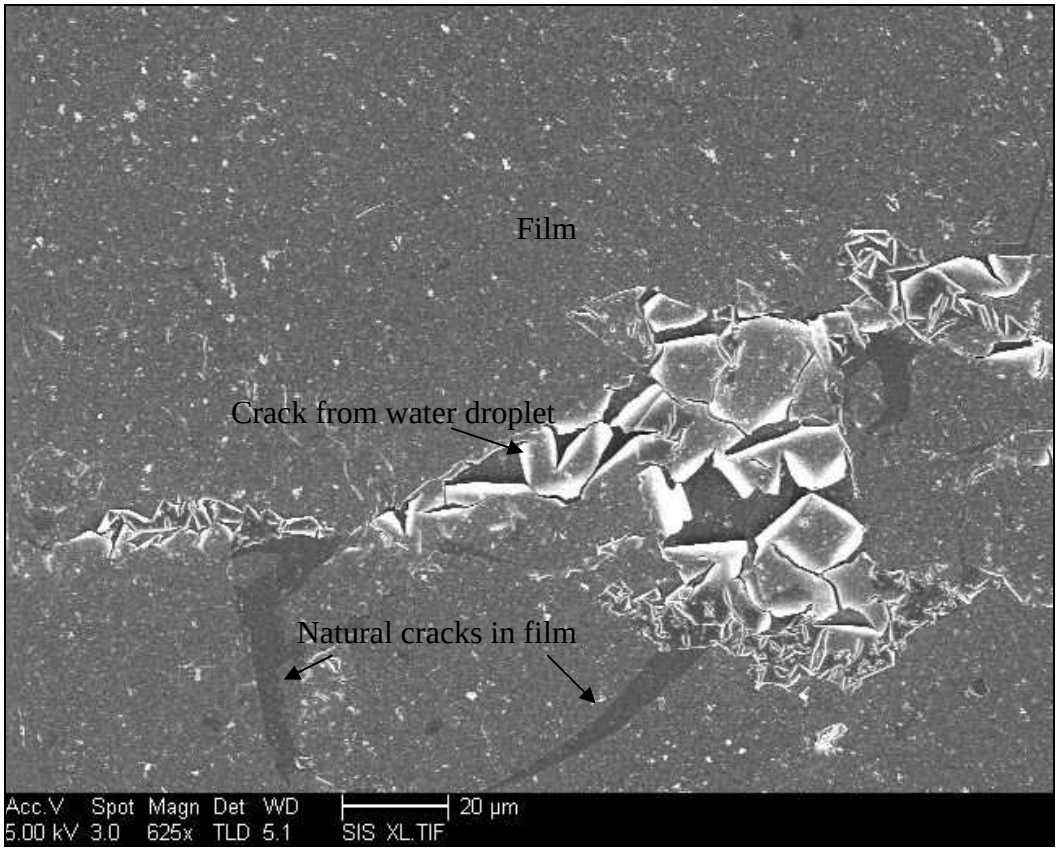

Figure 22. HRSEM micrograph of a Driftwood Creek film on a glass cover slip. Cracking and flocculent masses similar to those found in previous SEM work are visible, as well as more extensive cracking features.

Higher magnification of the flocculent indicates that sheath-like organisms are quite common (Figure 23). No similar structures were found in the film. Part of the flocculent was further enlarged, which provided insight to the texture of the material. The flocculent appears to be made of many filaments that have a biologic appearance.

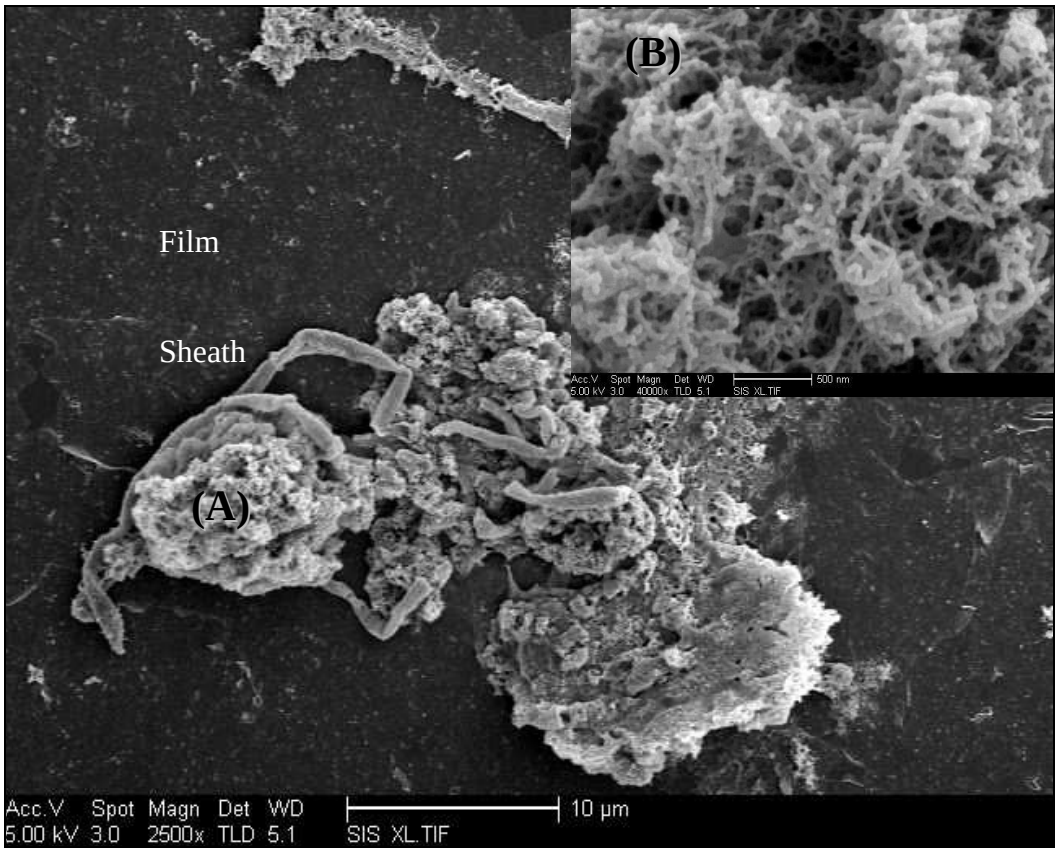

Figure 23. HRSEM micrograph of the flocculent. Sheath like features are visible and higher magnification of (A) (inset B) indicates the flocculent is made up of many small filaments.

The HRSEM-EDS was used to further constrain the amount of carbon in the film and flocculent. The sheath structures were too small to determine carbon content without influence of the film or flocculent. Carbon is present in both film and flocculent, although it appears to be slightly higher in the flocculent (Figure 24). Based on visual comparisons between peak heights of carbon and oxygen the film has a ratio of 3:14 carbon to oxygen while the flocculent has a ratio of 2:3 carbon to oxygen. Conditions that allowed for carbon analysis could not be used to accurately

detect the amount of iron in the film, so no comparison between carbon and iron, or any other constituent, can be made from these data.

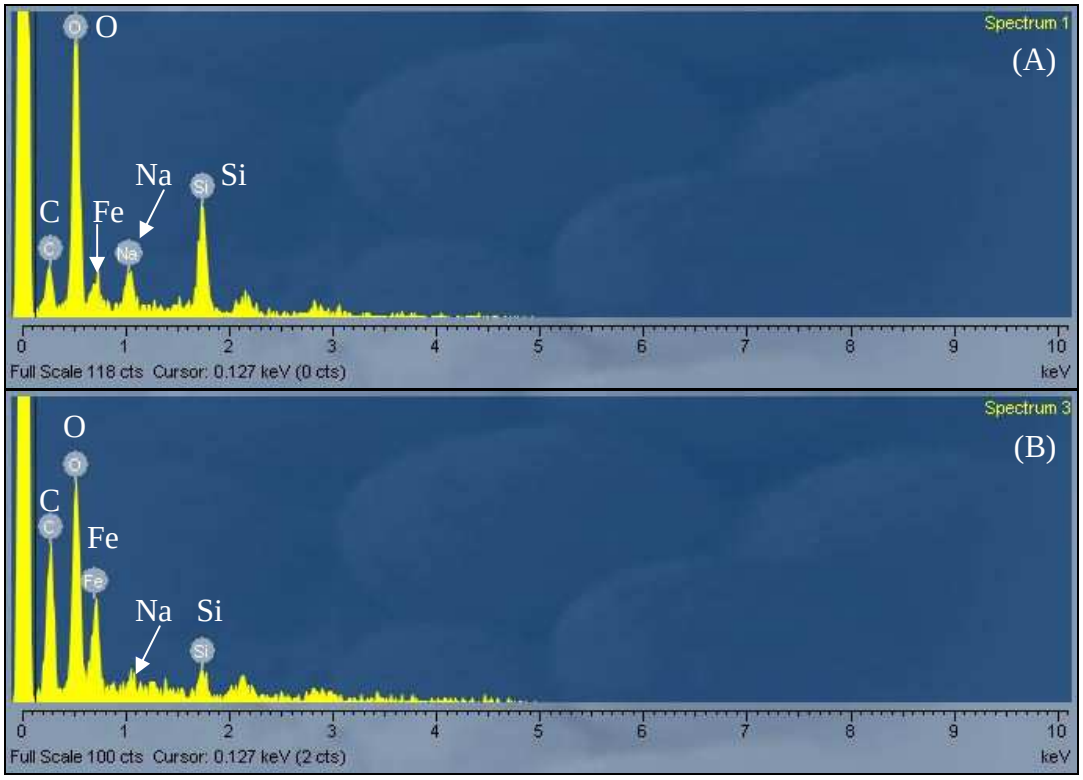

Figure 24. EDS spectra from samples analyzed with the HRSEM. (A) is the film itself, iron is the peak between oxygen and sodium. (B) is a spectrum from the flocculent.

X-ray Diffraction (XRD)

Three samples of film on QZB slides, including eight scraped samples, and two different sediment samples from the bottom of the pools, were analyzed by XRD. QZB1 and QZB2 are from Driftwood Creek and QZB3 is from Seal Rock. The scraped films are labeled with the site and date they were collected (Table 2).

Analysis of the films collected directly on the slides were too thin to be analyzed directly on the slide. Figure 25 shows a blank slide, scanned before the film was dipped onto it with an overlay of the same slide dipped in the film. There is no discernable difference between the two diffraction patterns.

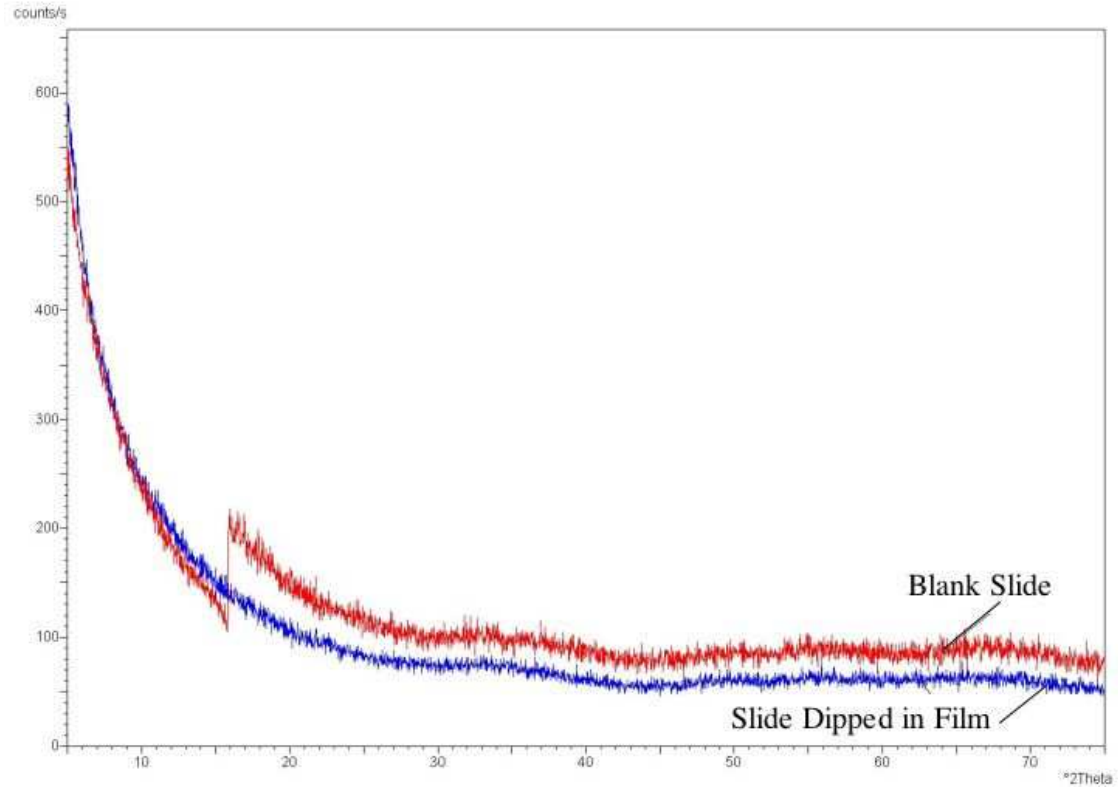

Figure 25. Cu Kα radiation XRD pattern of blank quartz zero background slide (blue) overlain by the same slide dipped in film (red) collected in November 2004 at Driftwood Creek. The jump in counts on the blank slide (blue) was a glitch in the detector. Without the jump the scans would be the same, the only difference being a slight offset in counts.

The scraped films indicate similar mineralogy of the films. Figure 26 shows a diffraction pattern of scraped film from Driftwood Creek collected in January 2005, which can be compared to Figure 27, a composite of films from Seal Rock. Scraped film from both sites were similar to each other, often containing two-line ferrihydrite

peaks around 2.6 and 1.5 Å. The 2.6 Å band may shift up to 2.8 Å or down to 2.5 Å while the 1.4 Å band ranges between 1.41 and 1.55 Å. A small poorly crystalline peak was found at 4.5Å. Quartz and halite were the two other mineral phases associated with the films. The halite likely comes from sea-spray while the quartz is likely from the beach sand in the surrounding environment.

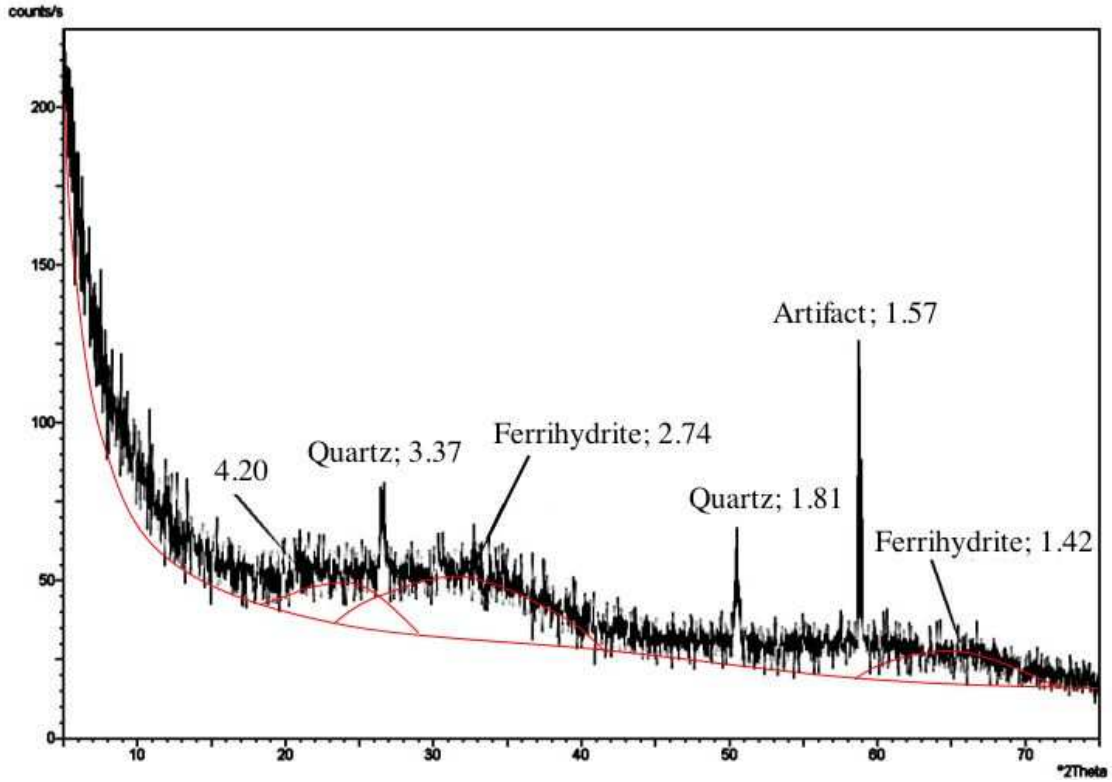

Figure 26. Co Kα radiation XRD pattern of scraped film collected in January 2005. two-line ferrihydrite (2.61 and 1.57 Å), quartz (3.37 and 1.81 Å), and a 4.5Å line are shown.

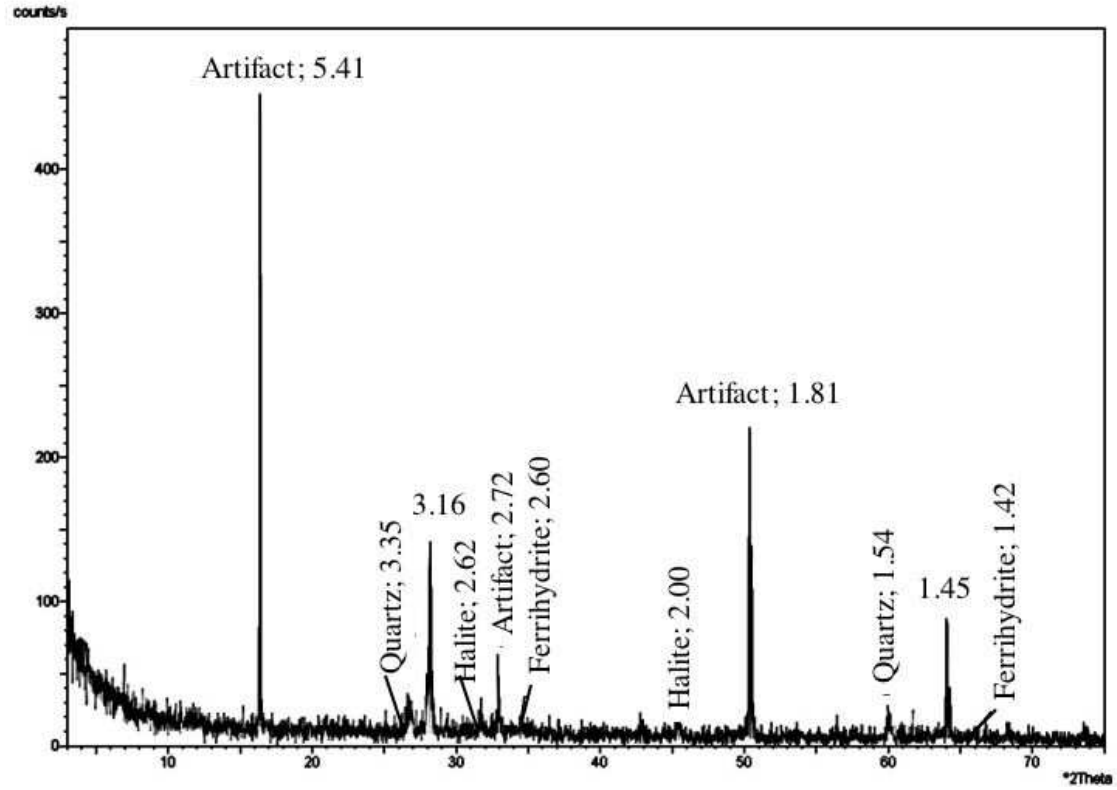

Figure 27. Cu Kα radiation step scan of a composition of scraped films from a Seal Rock seep pool.

Three artifact peaks were found in association with the QZB slides, 5.4, 2.7, and 1.8 Å. By turning the QZB slide 90° the peaks disappeared, indicating they were on the slides, not part of the sample. All QZB slides were run blank to insure the peaks were part of the slide and could be avoided. Not all samples were rerun in the new orientation; artifact peaks are labeled appropriately.

In addition to artifact peaks, some other peaks appeared that could not be attributed to known minerals. These peaks include a 1.63 Å peak, a peak between 1.57-1.56 Å, a 1.45 Å peak, and a peak between 1.33-1.32 Å. These peaks could not be tied to any distinct mineral phase, and so their origin remains unknown.

The flocculent from the bottom of the seep pools at Driftwood Creek was analyzed as well. It was found to be two-line ferrihydrite (Figure 28). These data are consistent with the findings of Johnson (2003), who also found two-line ferrihydrite in the flocculent. No 4.5 Å peak was found in the flocculent samples. Figure 29 is an unpublished reference pattern of ferrihydrite found at Driftwood Creek collected by Dr. John Baham of the Soil Sciences Department of Oregon State University prior to this study.

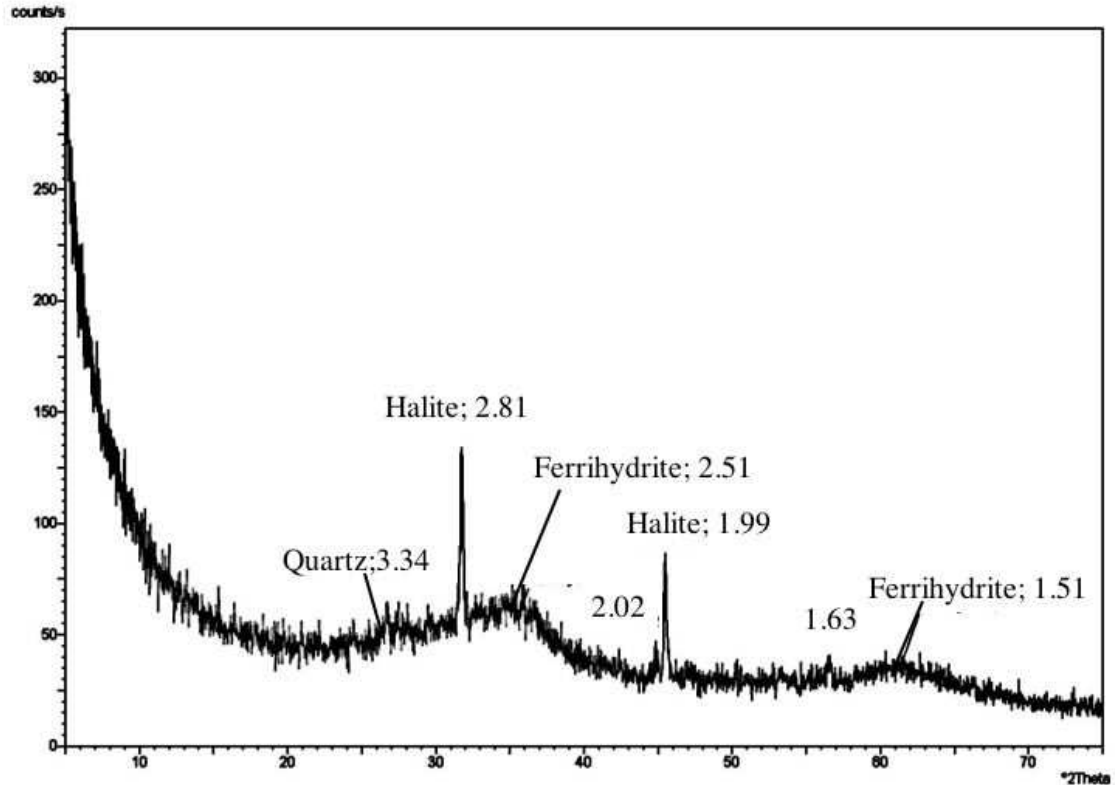

Figure 28. Cu Kα radiation XRD pattern of the flocculent found at the bottom of seep pools at Driftwood Creek.

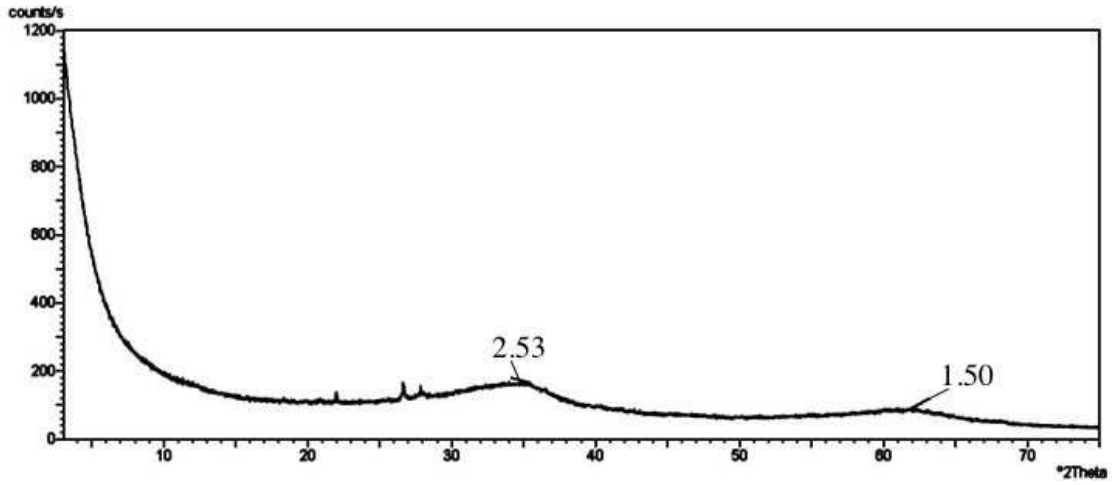

Figure 29. Cu Kα radiation XRD pattern of ferrihydrite as found in previously in Driftwood Creek seep pools by Baham (unpublished).

After XRD analysis was completed on a scraped film from Driftwood Creek the film was used for TGA analysis. XRD patterns before and after were collected to observe the changes in mineralogy. Before heating, the film contained two-line ferrihydrite and several of the peaks above 50 °2Theta (Figure 30). After heating the film to 950 °C it morphed into hematite and quartz (Figure 31), indicating that the film contains significant amounts of silica. The peaks at 1.46, 1.33, and 1.32 Å were not present after TGA analysis. They were either destroyed by the heating process or obscured by the hematite.

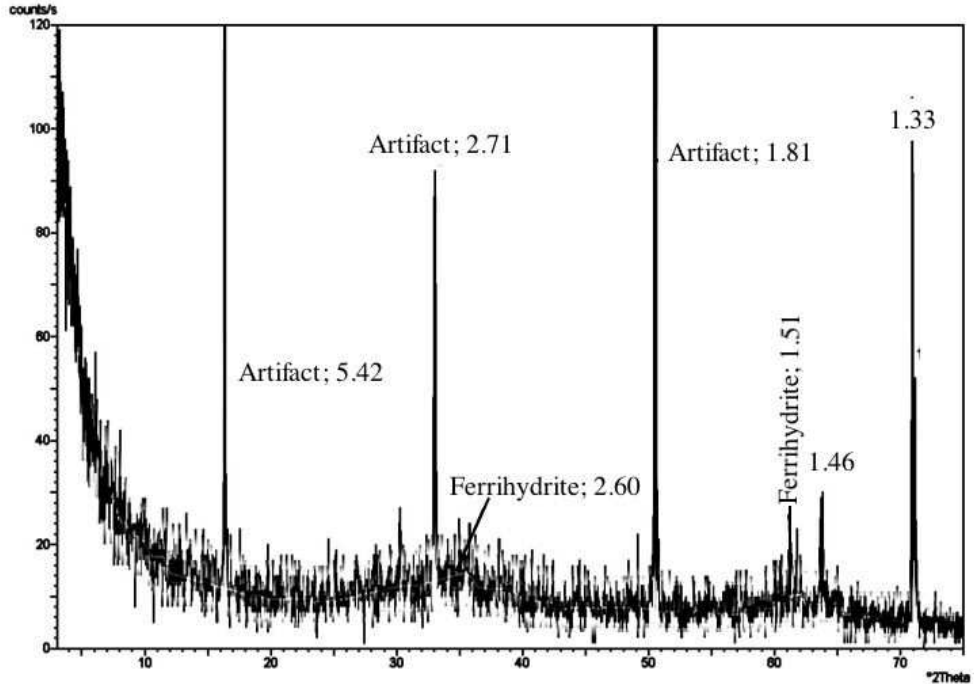

Figure 30. Cu Kα radiation XRD pattern of scraped films from Driftwood Creek seep pool prior to TGA analysis.

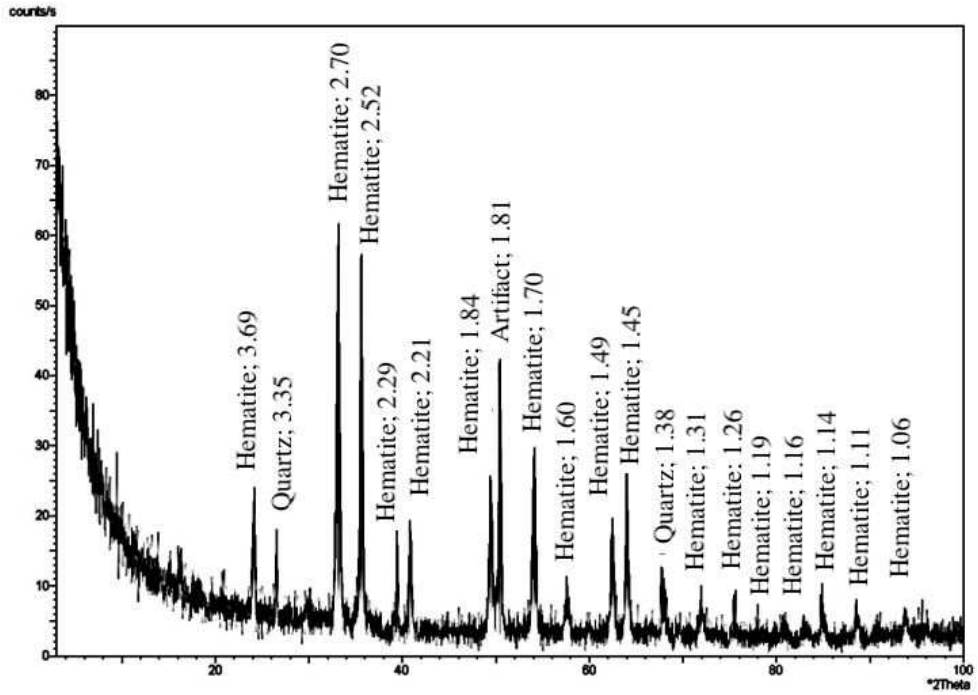

Figure 31. Cu Kα radiation XRD pattern of the film after TGA analysis.

Water Chemistry

At Driftwood Creek a total of 14 samples were collected from a shallow well and six seeps. One seep was sampled during each collection period, called Driftwood Creeks Spring (DCS). Several different seep pools were analyzed, labeled SeepX, where X is a date and number identifying when in the sequence of sampling it was collected. Some seep pools were sampled on multiple dates, in which case the date sampled follows the name. The Orcas well was located at the top of a small discharge stream. The well and seep samples are separated in sampling notation by well or seep. Samples were collected only from the well on 2/5/05, only from the seeps on 5/08/04, 8/31/04, 10/13/04, and 11/17/04, and from both the well and the seeps on 1/8/05, 1/22/05, and 2/5/05. Analytical methods included IC and ICP-AES.

Seep chemistry was obtained to better understand the environmental conditions under which the films form. The anion and cation concentrations are shown in Table 5 and Table 6, respectively. The pH, Eh, water temperature, total dissolved solids (TDS), and dissolved iron and oxygen are shown in Table 7. Dissolved iron and oxygen were measured using a CHEMets Test. All other measurements were made using a multifunction pH probe. TDS is a product of the conductivity and an empirical constant.

Table 5. Summary of anions found in Driftwood Creek water. Analysis by Nick Chambers and John Baham, Soil Science Department, Oregon State University.

Well	F^- ppm	Cl^- ppm	NO_3^- ppm	PO_4^{3-} ppm	SO_4^{2-} ppm
ORCA_010805	0.05	32.86	0.00	0.30	3.50
ORCA_012205	0.01	27.68	0.16	0.07	3.45
ORCA_020505	0.10	32.18	0.25	0.00	3.27
Seeps					
Driftwood 1 5/04	0.30	131	0.82	ND	0.38
Driftwood 2 5/04	0.11	63.5	0.18	ND	6.80
SEEP1_010805	0.11	97.68	0.02	0.07	20.44
SEEP1_012205	0.05	72.56	0.03	0.05	9.03
SEEP1_020505	0.13	98.54	0.39	0.00	7.34
SEEP2_012205	0.16	82.90	0.13	0.00	6.19

ND = Not Determined

Table 6. Cations analyzed by the AES and their concentrations. Analysis by Nick Chambers and John Baham, Soil Science Department, Oregon State University.

Well	Al^{3+} ppm	Ca^{2+} ppm	Fe_{Total} ppm	K^+ ppm	Mg^{2+} ppm	Na^+ ppm	Si^{2+} ppm
ORCA_010805	0.13	3.49	0.40	0.77	1.86	19.74	3.68
ORCA_012205	0.16	3.70	0.54	0.87	2.00	17.41	3.82
ORCA_020505	0.15	4.14	0.58	0.79	2.17	19.06	3.84
Spring/Seep							
HORCA_101304	0.16	4.28	5.45	1.32	3.02	23.08	4.79
HORCA_111704	0.16	4.30	5.52	1.39	3.43	26.68	5.00
HDCS_101304	0.11	4.56	1.53	1.67	3.88	30.84	5.91
HDCS_111004	0.11	4.96	1.19	1.56	4.18	34.28	5.86
HDCS_010805	0.17	4.02	2.57	2.54	3.44	42.06	5.20
SEEP1_010805	0.16	6.94	9.40	3.22	8.34	69.97	6.20
SEEP1_012205	0.14	5.30	3.56	3.20	7.34	50.29	4.47
SEEP1_020505	0.16	5.98	8.54	4.31	6.40	67.02	6.76
SEEP2_012205	0.16	6.85	8.77	3.69	7.36	69.03	7.04

Table 7. Meter readings for water sampling dates.

Well	Temp. (°C)	pH	Redox (mV)	Cond. (µS/cm)	TDS (ppm)	Dissolved Fe* (ppm)	Dissolved O* (ppm)
ORCA_010805	9.5	5.84	152	98.23	141	ND	ND
ORCA_012205	15.4	5.38	174	98.70	122	ND	ND
ORCA_020505	13.1	5.56	207	87.29	114	ND	ND
Spring/Seeps							
Spring_050804	ND	6.09	ND	ND	ND	ND	ND
Orca_083104	20.4	4.80	481	120	ND	8	0.2
Spring_101304	20.5	5.54	ND	ND	ND	ND	ND
Orca_101304	14.3	5.29	ND	ND	ND	ND	ND
Orca_111704	13.20	6.25	ND	ND	ND	7.5	0.7
Spring_111704	14.50	6.25	187	ND	ND	7.5	> 1.0
Spring_010805	7.60	6.70	226	195	ND	8	> 1.0
SEEP1_010805	5.50	6.68	241	318.04	507	> 10	> 1.0
SEEP1_012205	14.6	6.13	263	258.60	326	ND	ND
SEEP1_020505	12.1	5.87	255	300.40	403	ND	ND
SEEP2_012205	14.6	5.84	254	332.29	419	ND	ND

Cond. = Conductivity
TDS = Total Dissolved Solids
* = Determined by CHEMets Test
ND = Not Determined

The anions in the water at Driftwood Creek generally have higher concentrations in the seeps than in the well. Phosphate may be an exception with the well having concentrations up to 0.3 ppm while the seeps had 0.07 ppm. However, there are not enough samples to be sure of this trend. Dissolved fluoride concentrations are higher in the seeps, averaging 0.14 ppm, to the well levels of 0.5 ppm. Chlorine and sulfate are at least twice as high in the seeps than in the well, averaging 91 ppm compared to 31 ppm for chlorine and 8.4 ppm to 3.4 ppm for sulfate. The differences between the seeps and well are likely due to sea spray, which

is added to the exposed seeps at higher rates than to the well. Nitrate is only slightly higher in the seeps, 0.26 ppm, than in the well, 0.21 ppm.

The cations show a similar trend to the anions. Aluminum is the only cation that is consistently similar between well and seeps with concentrations around 0.15 ppm. The average calcium concentration is higher in the seeps, 5.26 ppm, almost twice as much as the average concentration in the wells, 3.77 ppm. The potassium average is three times higher in the seep, 2.65 ppm, than in the well, 0.8 ppm. Sodium averages are similar, 18.73 ppm in the wells to 47.73 ppm to the seeps; sea spray is a likely cause of the higher sodium in the exposed seeps. Magnesium levels in the seeps average 5.5 ppm, about twice as much as in the well, which averages 2.0 ppm. Silica averages are similar, with a concentration of 5.73 ppm in the seeps and 3.78 ppm in the well.

The average iron concentrations are much higher in the seeps than in the well, 5.4 ppm to 0.51 ppm, respectively. In the winter, where well data are available, there is upwards of twenty times more total iron in the seeps than in the well. Conditions at this time favor the presence of Fe(II) with Eh below 400 mV and pH below 6. This increase in iron between the well and the seep is due to plant and soil horizons through which the groundwater must travel.

Two winter sampling dates from Driftwood Creek provided inorganic and organic carbon data for the seeps and wells. The dissolved inorganic carbon (DIC) was consistently higher than the dissolved organic carbon (DOC) for both seeps and

wells. The seeps had at least twice and up to seven times as much carbon than the wells. Carbon data are summarized in Table 8.

Table 8. Dissolved carbon data for Driftwood Creek well and seeps.

Well	DOC (µM)	DIC (µM)
ORCA_010805	206.1	379.4
ORCA_012205	325.8	392.5
Seeps		
SEEP1_010805	1017.8	1601.9
SEEP1_012205	755.6	959.8
SEEP2_012205	1133.3	2884.7

DOC = Dissolved Organic Carbon
DIC = Dissolved Inorganic Carbon

Well data are only available in the winter and show lower concentrations of anions and cations than data from the seeps (Table 5 and Table 6). The well, located just above bedrock, picks up water of a deeper flow path that has been exposed to fewer nutrients from plants and human influences. Seeps are made up of water that flows through a shallower path exposed to plants, soil and human influences. Figure 32 is a sketch of the movement of water in the area.

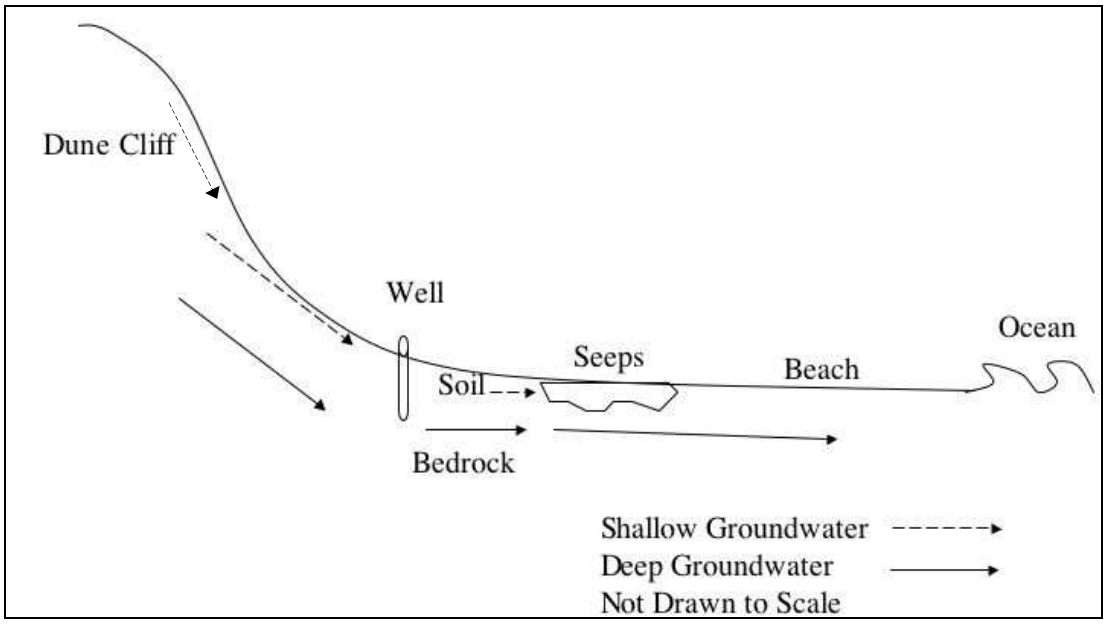

Figure 32. Groundwater movement at Driftwood Creek.

Differences observed in the seeps between the dry and wet seasons may be explained by the amount of water present in the system. Concentrations are higher in the winter due to more rainwater entering the groundwater system and picking up nutrients. In the summer concentrations are lower because there is not enough water movement to remove as many ions from the soil. Anomalies, such as the chlorine and sulfate in the seeps in May 2004 (Table 5), may be explained by human contamination such as water treatment and septic systems.

Fe(II)/Fe(III) ratios

The oxidation state of iron of the iron-bearing films was determined colorimetrically via the 1,10-phenanthroline method (Loeppert and Inskeep, 1996). Samples were collected on February 5, 2005 on glass fiber filter paper and placed in

22 mL of HCl. In one milliliter of water the concentrations of Fe(II) ranged from 0.12 ppm up to 2.47 ppm while the concentration of Fe(III) ranged from 3.76 to 12.21 ppm. Total iron ranged from 3.9 to 14.7 ppm. Samples 1 and 4 were coated with film as completely as samples 2 and 3, causing the large range in the concentrations. The ratio of Fe(II):Fe(III) is about 0.2. Table 9 shows the values for 1 mL of the water as well as for the whole bottle collected.

Table 9. Fe(II)/Fe(III) ratios in the iron-bearing film determined colorimetrically from samples collected 02/05/05 at Driftwood Creek.

	Fe(II) (ppm)	Fe(III) (ppm)	FeTOT (ppm)	Fe(II) (mg)	Fe(III) (mg)	FeTOT (mg)
	Analysis of 1mL			mg on Filter		
Filter Blank	0.00	0.00	0.00	0.00	0.00	0.00
Filter Blank	0.00	0.00	0.00	0.00	0.00	0.00
Filter Blank	0.00	0.00	0.00	0.00	0.00	0.00
Seep1 - 1	0.13	5.22	5.35	0.01	0.12	0.12
Seep1 - 2	2.47	12.21	14.67	0.05	0.27	0.32
Seep1 - 3	1.84	8.93	10.77	0.04	0.20	0.24
Seep1 - 4	0.12	3.76	3.88	0.01	0.08	0.09

From the concentrations in Table 9 it has been determined that about 17% of the film is Fe(II) and 83% is Fe(III). Up to 14% of the Fe(II) may have come from the water. It is estimated that the filter papers picked up at most 1 mL of water along with the film during sampling. The concentration of total iron in the pool that day was about 8 ppm, or 8 µg/mL, most of which was likely Fe(II). Therefore the filter paper may have collected up to 8 µg/mL of Fe(II) from the water, which is 14% of the Fe(II)

collected in the film. The remainder of the Fe(II) must be part of the structure of the film.

Thermogravimetric Analysis (TGA)

TGA results showed a curve with a water loss followed by two larger weight losses. The total weight loss was 22.7%. The first loss of 1.9% occurred between 70 and 100 º C and is atmospheric water. The next loss, likely structural water or OH bonds, was around 130 to 200 ºC, where the sample lost another 7.1%. The final loss occurred between 340 and 360º C and it represented the remaining 14.4% of the lost weight. This last step represents the loss of structural OH and it reflects the final dehydration stage between the two mineral phases. Figure 33 shows the weight loss compared to the temperature. Iron oxides with structural OH lose weight between 250 and 400 °C (Cornell and Schwertmann, 2003).

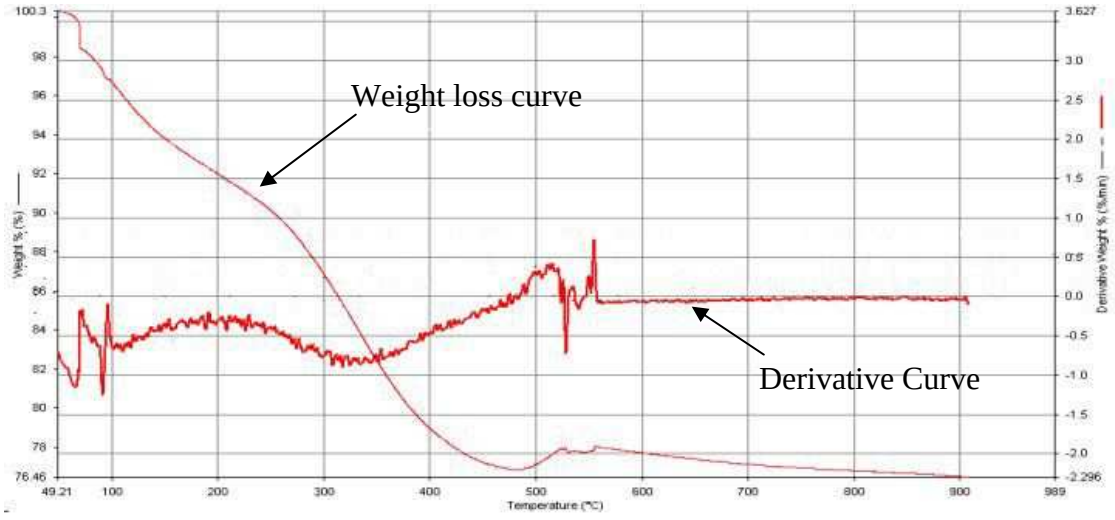

Figure 33. Results of TGA performed on several compiled films from Driftwood Creek.

Depending on the formula for ferrihydrite that is used, the 22.7% loss is similar to what one would expect with ferrihydrite changing into hematite (Fe_2O_3). Cornell and Schwertmann (2003) use the formula $Fe_5HO_8{\cdot}4H_20$, updated from $Fe(OH)_3$. These ferrihydrite formulas loose 16.9% and 25.3% respectively as they change to hematite. Based on SEM, TEM, and Fe(II)/Fe(III) ratios a chemicial formula of $Fe^{2+}_{0.43}Fe^{3+}_{1.72}(OH)_6$ is proposed for the film. This formula has a 12% weight difference between hematite and ferrihydrite. This formula does not take carbon into consideration as the exact role it plays in the structure of the film is still unclcear.

It was hoped that TGA would provide insight to the carbon content of the film. However, the graph is inconclusive around 500 °C where the expected carbon loss should take place. This is likely due to the small amount of sample used in analysis. Some carbon is contained in the film, and the third weight loss between 340 and 360º C may represent some carbon loss (Campbell et al., 2002).

Density of the Film

The iron-bearing film is lightweight, i.e. five 2.5 cm by 4.5 cm microscope slides covered in film yields about 2.2 mg. With an estimated thickness of 100 nm this would give the film a density of 3.9 g/cm^3. The density of ferrihydrite is 3.8 g/cm^3 (Barthelmy, 2005).

Fourier Transfer Infrared Spectroscopy (FTIR)

Conventional transmission, transmission and reflectance modes using the infrared microscope, and at a grazing angle of 85° specular reflectance accessory were used. Conventional transmission spectra produced the best patterns, characterized by strong, but broad, absorption bands. Transmission spectra of Sample 2, collected from Driftwood Creek Spring November 17, 2004 (Figure 34), exhibits a strong and very broad OH absorbance band from 3700 to 2900 cm^{-1} and broad bands in the fingerprint region (1800 to 500 cm^{-1}).

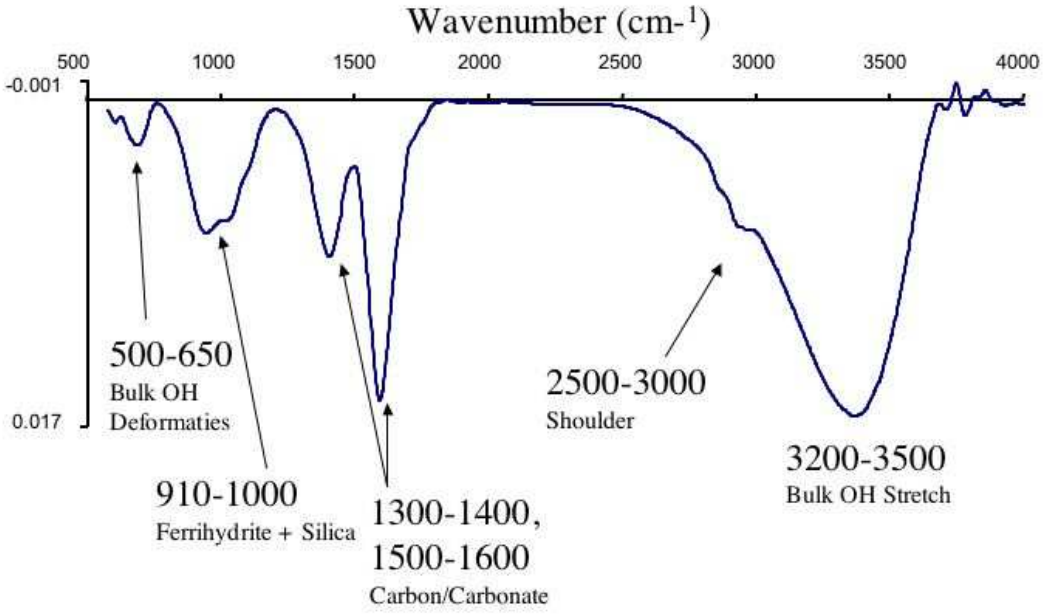

Figure 34. FTIR Transmission spectra of Sample 2. Bulk OH deformities are seen in the 500 – 650 cm^{-1} range while bulk OH stretches are between 3200 and 3500 cm^{-1}. The band between 910 – 1000 cm^{-1} is similar to ferrihydrite and silica. Carbon and/or carbonate are shown with the two bands 1300 – 1400 cm^{-1} and 1500 – 1600 cm^{-1}. A shoulder of unknown origins occurs in the 2500 – 3000 cm^{-1} range.

The absorption bands in the fingerprint region show similarities to ferrihydrite. Cornell and Schwertmann (2003) indicate the free surface OH groups are broad in two-line ferrihydrite, with peaks around 3615 cm^{-1} and 3430 cm^{-1}. Bands at 650 cm^{-1} are bulk OH deformities and ferrihydrite with a few percent silica are described at 940 cm^{-1}. Seehra et al. (2004) also find silica substitutes producing bands at 942 cm^{-1} and 1018 cm^{-1}, again similar to the pattern of the sample from Driftwood Creek.
The peaks higher in the fingerprint region are likely due to carbon bonds. Absorption bands at 1589, 1402, and 1018 cm^{-1} may be attributed to the C=C stretch, the =CH2 deformation, and the =CH wag, respectively (P. Gassman, Written Communication, May 2005).

High Resolution Transmission Electron Microscopy (HRTEM)

Two HRTEM grids were analyzed; one grid was dipped twice in the film, the other only once. The single dipped film was found to be of suitable thickness (around 100 nm) and the other, while thick in some places, was also suitable.

Primary HRTEM electron diffraction indicated some dried salts on the grids, identified by the cubic nature of the electron pattern. Energy filtered electron diffraction patterns indicate the film is amorphous, with rings at 4.5 Å, 2.5 Å, and 1.4 Å (Figure 35), in some places the diffraction pattern shows only the latter 2.5 and 1.4 Å rings (Figure 36). These rings are consistent with both the standard ferrihydrite pattern (Cornell and Schwertmann, 2003), and the XRD patterns produced in this study.

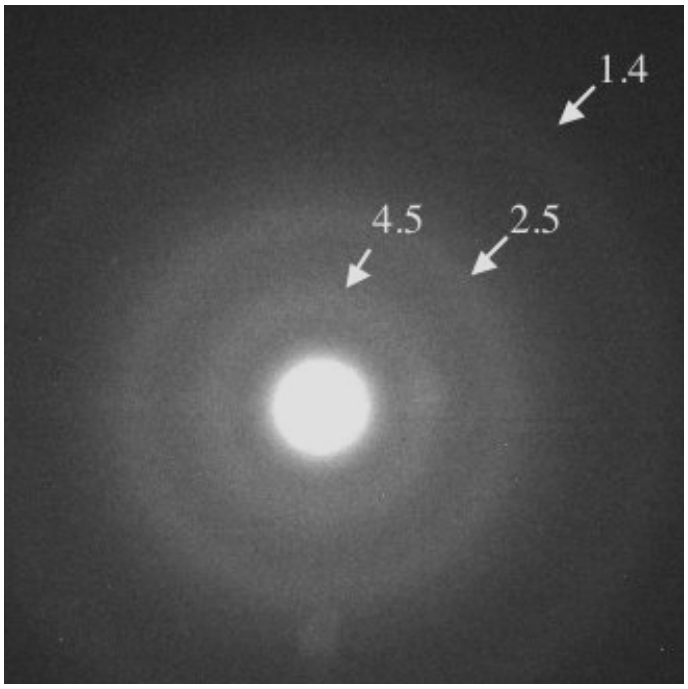

Figure 35. TEM diffraction pattern of iron-bearing film showing three rings of the film.

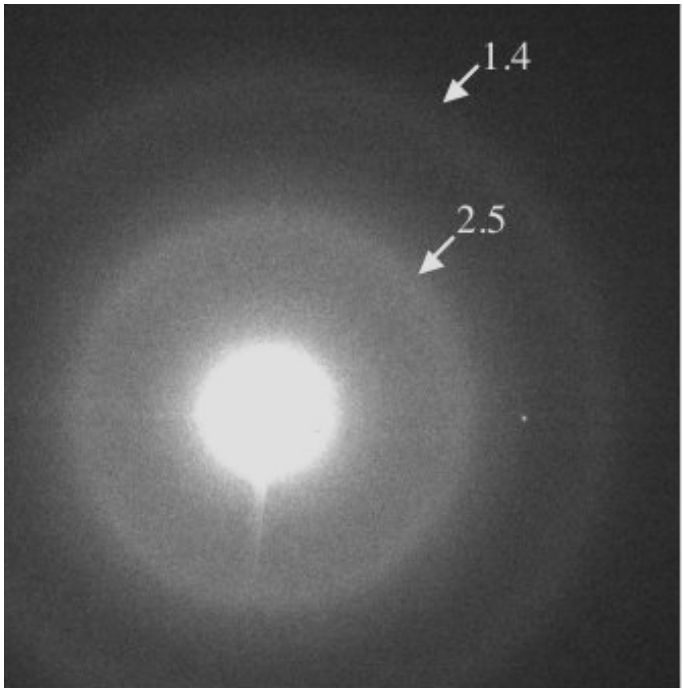

Figure 36. TEM diffraction pattern of two ring spectra on the iron-bearing film

D-spacings were determined using a curve fitting method developed by Dr. Rick Hugo. A circular integration of the diffraction patterns was generated to determine the radius and normalized radius from the center of the pattern. The data were then curve fit and the peaks were modeled as a wave function (Figure 37). This provides the height and width of the peaks.

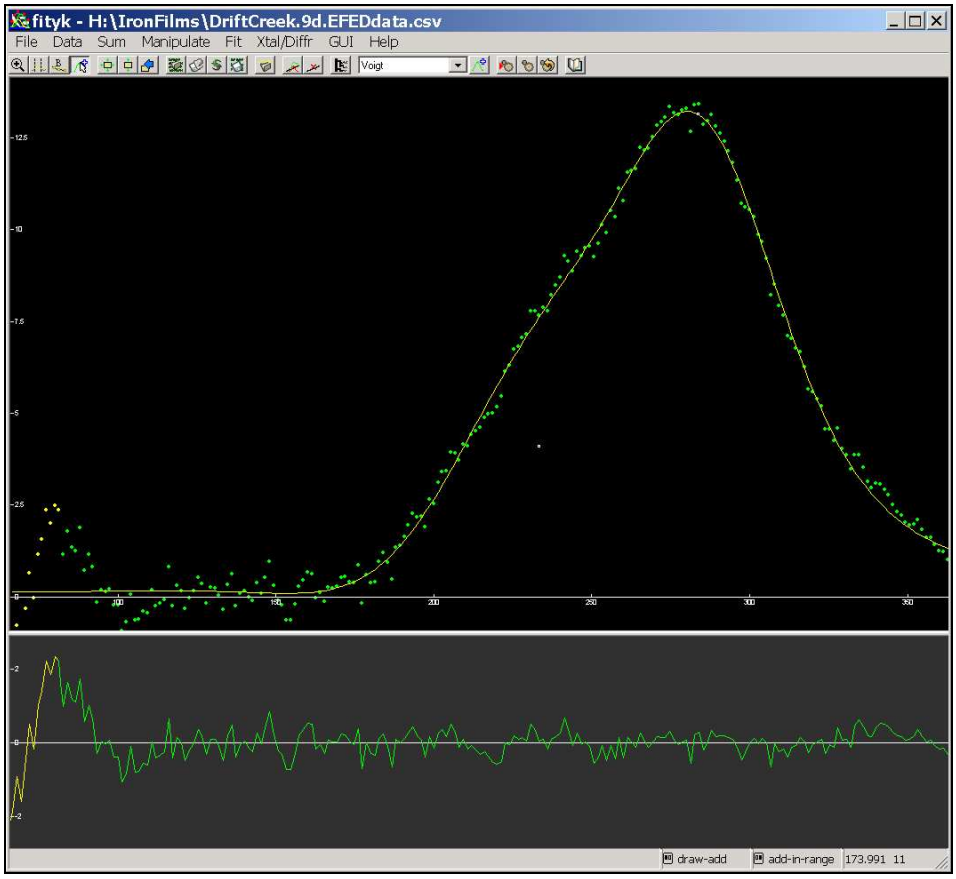

Figure 37. Curve fitting graph used to determine the d-spacings of the rings of the TEM diffraction pattern. The upper frame is the curve fitting and the bottom frame is how well the points correspond to the fit.

Bright-field images provided further insight to the morphology of the film (Figure 38). The platy surface of the film is variable, with darker and lighter speckled areas. The speckling indicates the thickness of the film. Overall the film is made of the same material, but with varying compositions, which reflect different thicknesses. Cracks, similar to those found in SEM analysis are present.

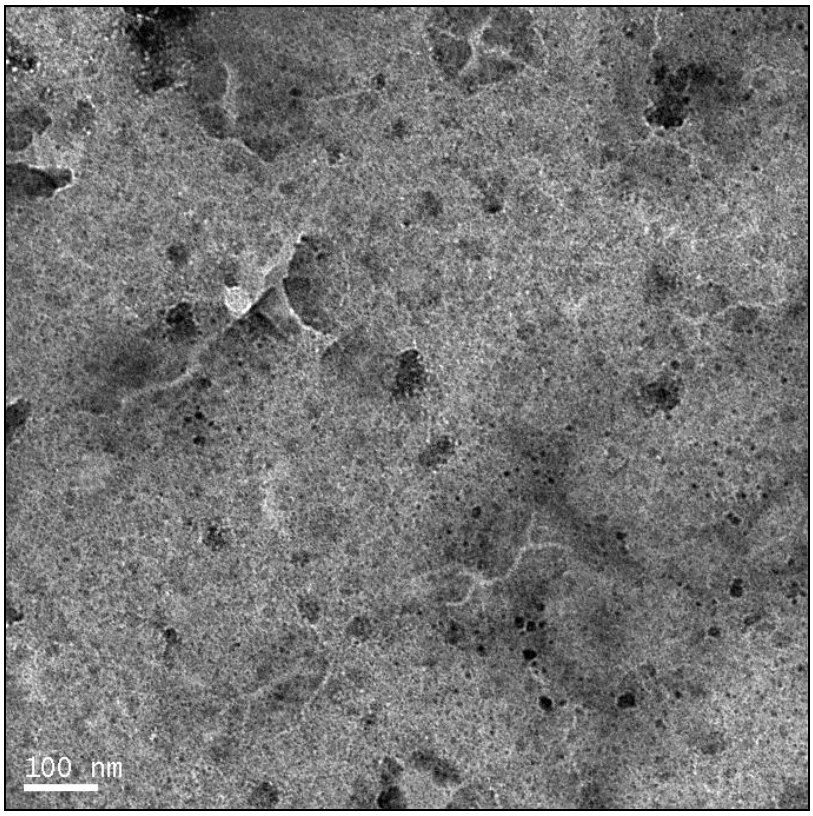

Figure 38. Bright-field image of iron-bearing film in the TEM.

Element maps taken of smaller sections of Figure 38 indicate areas of higher concentrations of carbon or iron. Figure 39 is an elemental map of the carbon in the films. The films were coated in carbon, as indicated by the light gray color of the overall map, however, the white circles distributed throughout the map reflect the film

environment. These uniform circles are in a different plane than the film itself, evidence that they are not part of the film and adhered to the film or the grid during collection. Figure 40 is an elemental map of the iron in the films. This map is darker than the carbon map, but light enough to indicate the presence of iron throughout. There are darker areas where there are iron deficiencies and lighter areas where the iron is more concentrated.

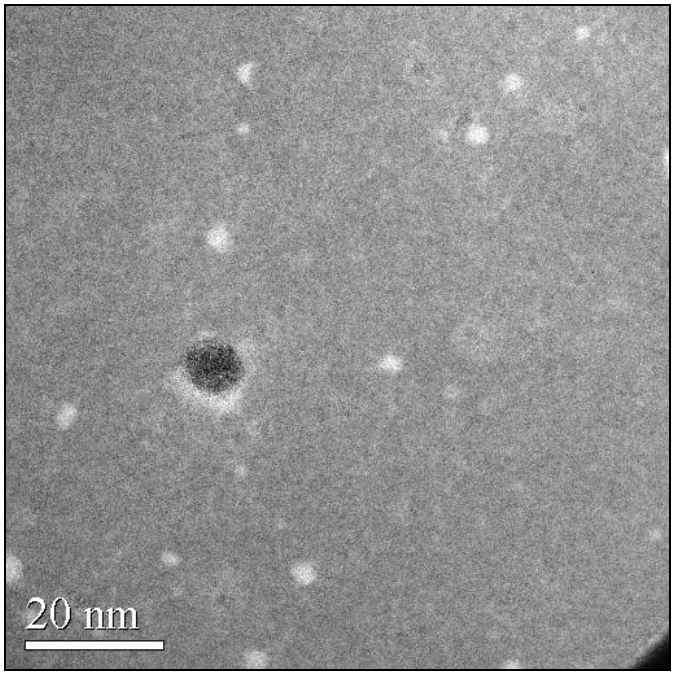

Figure 39. TEM element map of the carbon on the iron-bearing film.

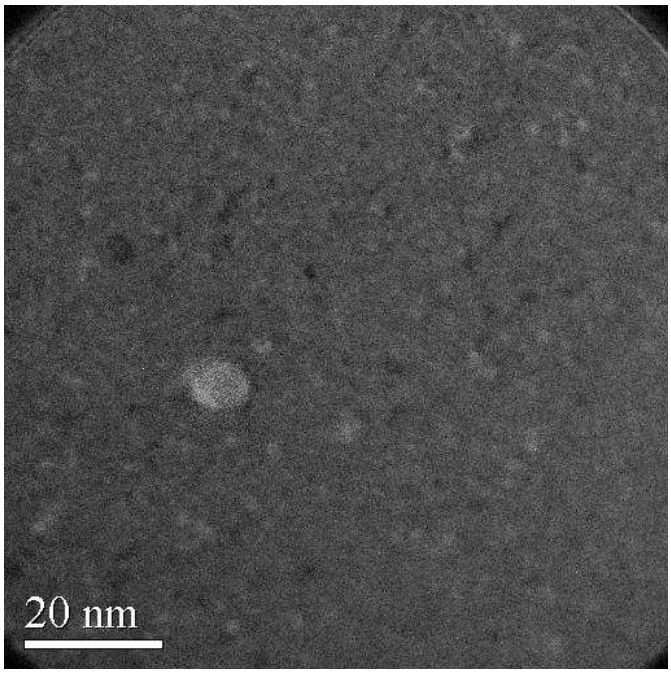

Figure 40. Elemental map from the TEM of the iron in the iron-bearing films.

In addition to elemental maps, parallel electron energy loss spectroscopy (PEELs) was used to look at the levels of elements in the section of the film that had two rings. SEM-EDS spectra helped to select the elements to analyze. The presence or absence of carbon, iron, oxygen, and silica was determined. Chlorine was not determined as this film was from Driftwood Creek where chlorine is not a major constituent. Figure 41 shows the carbon spectra. As mentioned previously, the grids were coated in carbon before being analyzed, but this carbon pattern is different from a sample containing no carbon, indicating that some carbon was also collected with the films. Figure 42 shows the iron peaks in the pattern. Figure 43 shows the oxygen, an element the SEM-EDS was unable to provide. While PEELs analysis does not indicate any silica (Figure 44), SEM-EDS indicates that there is more silica in the

samples than can be accounted for in the substrates. XRD analysis also finds silica associated with the film. The silica may be associated with the 4.5 Å ring. The PEELs spectrum was taken from a section of the film containing only two rings, not the third 4.5 Å ring, which again indicates that the film is not homogeneous.

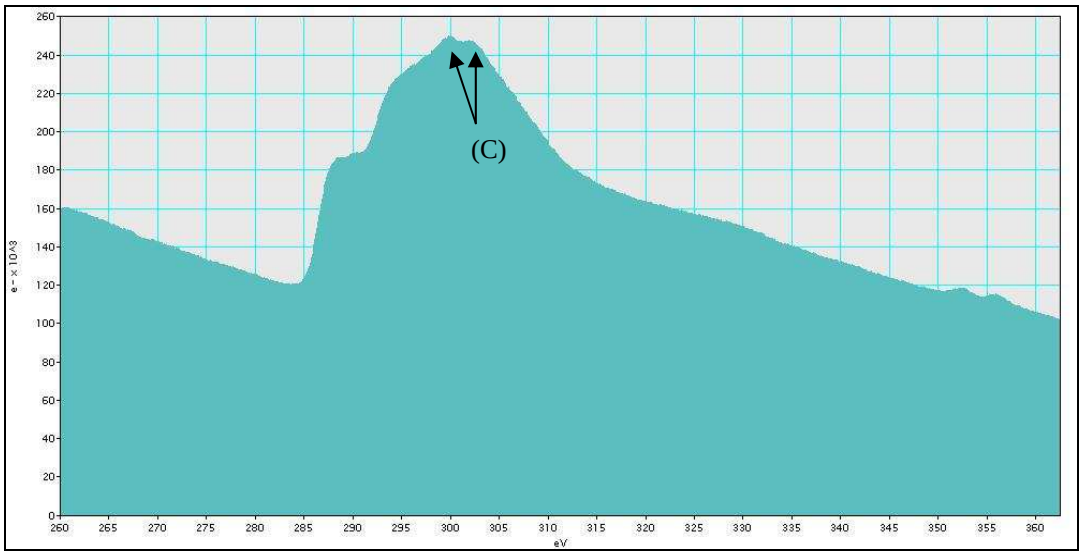

Figure 41. Carbon PEELs map of iron-bearing film. Peaks that are not part of the carbon coating (graphite) or the amorphous carbon gird are marked (C).

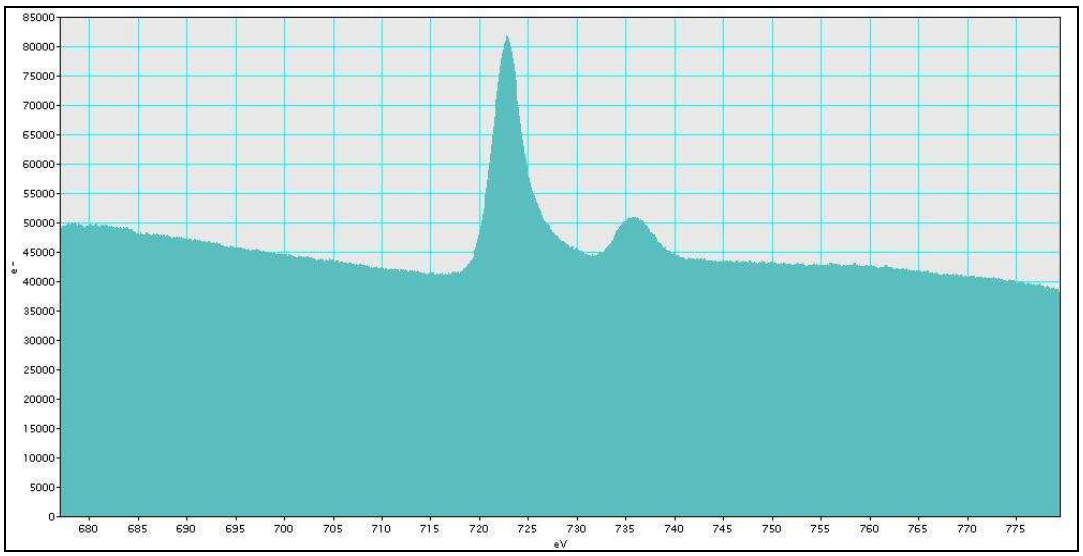

Figure 42. Iron PEELs map of iron-bearing film.

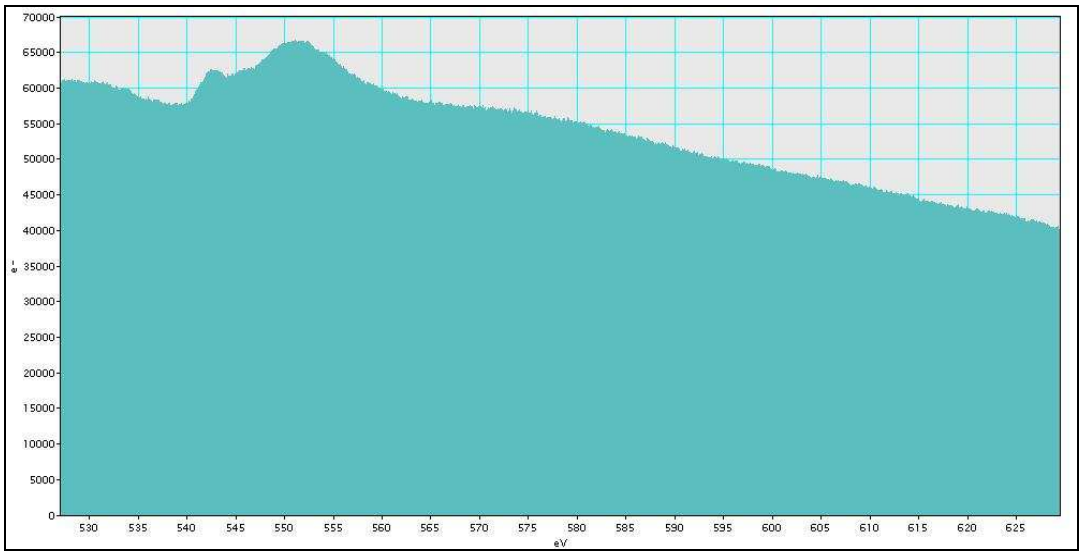

Figure 43. Oxygen PEELs map of iron-bearing film.

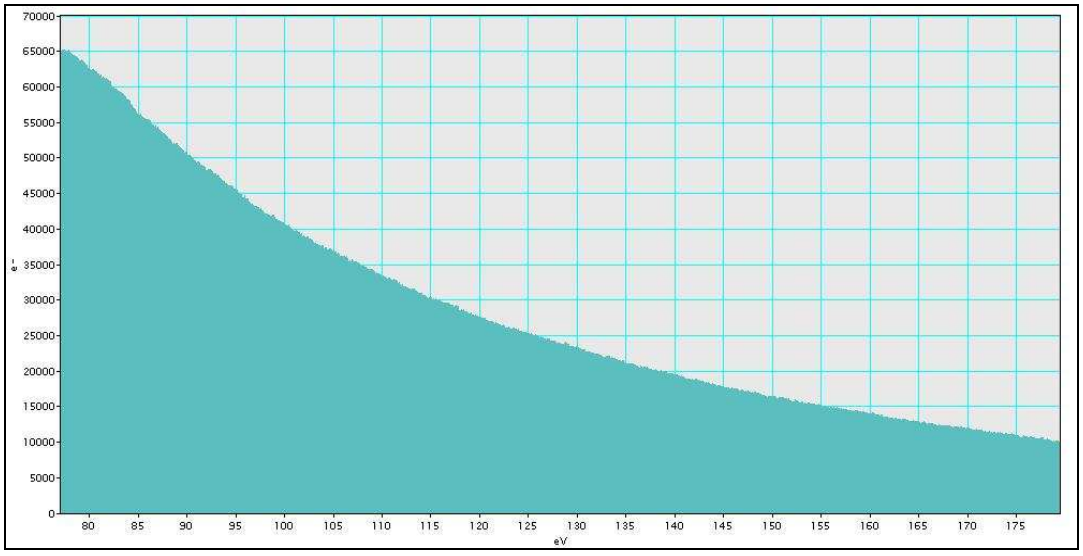

Figure 44. Silica PEELs map of the iron-bearing film. No silica was found in this part of the sample.

DISCUSSION

This study finds the iron-bearing films to be different from other films and minerals. To distinguish it from these other films I have named it Schwimmeisen, German for floating iron.

The focus of this section will be a discussion of the composition of Schwimmeisen as well as how it forms and why it floats. The first section will focus on the similarities and differences of Schwimmeisen to ferrihydrite. The second section will discuss how ferrihydrite most commonly forms. The third section will describe the difference between biotic and abiotic formation processes and compare Schwimmeisen to biofilms. Finally, the floating properties of Schwimmeisen will be examined.

Ferrihydrite – Similarities and Differences

Various analytical methods indicate some similarities and differences between Schwimmeisen and published data on two-line ferrihydrite. The similarities include XRD and TEM lines around 2.5 Å and 1.47 Å, as well as the presence of iron, oxygen, and some silica. Major differences from ferrihydrite include a 4.5Å line and the mixed valence of the film. Johnson (2003) identified the flocculent found below the films as two-line ferrihydrite, which this study finds to form from the further oxidation of Schwimmeisen.

TEM and XRD show that two-line ferrihydrite is present in Schwimmeisen. However, both methods also show a third line with a d-spacing of 4.5 Å. This third

line does not appear in every XRD scan or in all locations on the TEM grid. The d-spacing of the two-line ferrihydrite in this study is not always consistent with the 2.5 Å and 1.47 Å bands described by Cornell and Schwertmann (2003). In this study the 2.5 Å band may shift up to 2.8 Å while the 1.4 Å band wavers between 1.41 and 1.55 Å. This range is consistent with Vempati and Loeppert (1989) who find that if the silica to iron ratio is greater than 0.1 the lines may shift as much as 0.3Å.

SEM analysis indicates the presence of silica in Schwimmeisen. Seehra et al. (2004) show the affects of silica during synthesis of ferrihydrite (Figure 45). The XRD results of their two-line ferrihydrite gets broader as more silica is added. The XRD patterns from Schwimmeisen from Driftwood Creek and Seal Rock closely resemble the patterns Seehra et al. (2004) get when they use x = 0.5 Si/(Si+Fe) ratio. Si:Fe ratios from SEM-EDS from Driftwood Creek average 0.25 Si/(Si+Fe) ratio while samples from Seal Rock average a 0.4 Si/(Si+Fe) ratio. While the Si/(Si+Fe) ratios of this study are less than x = 0.5 the patterns are similar to results from Seehra et al. (2004), suggesting the ferrihydrite phases observed in this study are natural versions of what has been synthesized.

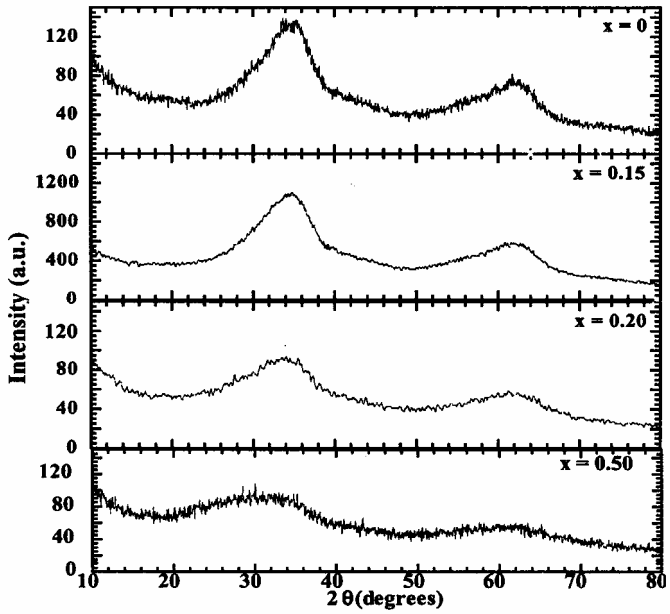

Figure 45. X-ray diffraction patterns of ferrihydrite with various compositions of x = Si/(Si+Fe) under a Cu K_α source (Seehra et al., 2004, used with permission).

As in the study by Seehra et al. (2004) the silica changes the XRD pattern from that of synthesized ferrihydrite. Campbell et al. (2002) also looked at the effects of silica on ferrihydrite, using differential thermal analysis (DTA) to determine how silica effected the transformation of ferrihydrite into hematite. They found that pure ferrihydrite has a significant change at 340 °C, whereas x_{Si} = Si/(Si+Fe) = 0.27 raises the transition temperature to 740 °C. As mentioned previously, SEM-EDS indicates that there is x_{Si} = 0.25 at Driftwood Creek where the TGA sample was collected. TGA data for this study find that there is a significant change at 360 °C with no reliable information above 500 °C. This change is not enough to suggest that our data matches Campbell et al.'s study.

Schwimmeisen is found to have an Fe(II) to Fe(III) ratio of 0.2. True ferrihydrite contains only Fe(III), while mixed valence oxides, green rusts or $Fe(OH)_2$, have a ratio ranging from 0.8 to 3.6 (Cornell and Schwertmann, 2003). Green rust also incorporates other anions into its structure, usually chlorides or sulfates. This divalent characteristic may have something to do with the 4.5Å line found in XRD and TEM analysis.

Laboratory experiments that produced green rusts (Benner et al., 2002) indicated that some bacteria may be crucial in the synthesis of this unique valence. Benner et al. (2002) put ferrihydrite in an anoxic water column with *Shewanella*, an iron-reducing bacteria. Over the next ten days the ferrihydrite turned into magnetite and green rust. They suggest that green rust may be a meta-stable mineral phase from the reduction between the ferric oxide and the ferrous oxide, similar to ferrihydrite as an intermediate phase of ferric iron before goethite formation. This mixed-valent mineral may be an intermediate between ferrous oxides and ferric oxides.

The mixed-valent nature of Schwimmeisen could also be an indicator that the film itself originates as pure ferrous iron. This is unlikely because Schwimmeisen forms at the water-air interface where the kinetics of the oxidation of ferrous iron in solution do not promote long residence times at the surface. However, ferrous species such as $Fe(OH)_2$ have similar XRD peaks at 2.4 Å and 1.6 Å but is a more crystalline phase than ferrihydrite (Miyamoto, 1976). Bernal et al. (1959) also studied $Fe(OH)_2$. This white precipitate is sensitive to oxygen, but is stable enough to allow the Fe^{3+} content to reach 10% of the total iron. Between the XRD patterns, which do not

include the other characteristic peaks of $Fe(OH)_2$, and the Fe^{3+} content, it does not seem likely that Schwimmeisen is formed from a reduced species of iron.

Schwertmann and Friedl (1998) used Mössbauer analysis to identify mixed-valent films in ferriferous streams. In this environment oxygen-rich groundwater starts oxidizing the iron in the stream. Goethite and ferrihydrite have been positively identified by Mössbauer analysis. The pebbles that these films were found on are of iron-free, lithologies. They are found at the bottom of streams unlike Schwimmeisen which is found at the water surface.

FTIR analysis shows Schwimmeisen has OH bonds and some, but not all, peaks associated with ferrihydrite. Cornell and Schwertmann (2003) describe ferrihydrite bands at 3615 cm^{-1}, 3430 cm^{-1}, 650 cm^{-1}, and 450 cm^{-1} with an additional band at 940 cm^{-1} for ferrihydrite with a few percent silica. Absorption bands found in the Driftwood Creek samples include a broad OH stretch between 3200 and 3500 cm^{-1}, a band between 500 and 650 cm^{-1}, and overlapping band between 900 cm^{-1} and 1000 cm^{-1}. The FTIR spectra are not resolved well enough to independently establish Schwimmeisen mineralogically. However, the OH bonds are consistent with a ferrihydrite phase.

Vempati and Loeppert (1989) studied ferrihydrite with silica. In their FTIR analysis they found a 990 cm^{-1} peak. This peak is consistent with the double peak found in the Driftwood Creek film sample. The double peak could suggest that there is both two-line ferrihydrite and ferrihydrite with extra silica.

FTIR of Schwimmeisen also has two peaks that do not appear in the published literature for ferrihydrite. These peaks occur at 1350 cm^{-1} and 1550 cm^{-1} (J. Cuadros, Personal Communication, June 2005). They might correspond to carbon and/or carbonate, associated with the pool environment where the film was collected. The amount of carbon present in Schwimmeisen is a constituent that this study has been unable to fully characterize.

Under both the optical microscope and the SEM Schwimmeisen is seen with two different morphologies: the film by itself and flocculent attached to the film. Under the optical microscope Schwimmeisen is clear or slightly brown, in places pieces of the flocculent are attached to it (Figure 15). Under the SEM Schwimmeisen is a platy, medium-grey with low topography, while the flocculent is brighter white and it displays a more stringy appearance (Figure 19). These two morphologies and their overlapping associations lead me to the conclusion that Schwimmeisen is a transitional phase that develops into the ferrihydrite flocculent. HRSEM seems to further support this theory, with bacteria only being found on the flocculent (Figure 23).

An experiment was conducted at Driftwood Creek to establish the rate of formation of Schwimmeisen. A hole was dug in the sand near where the films occurred on natural seeps. Due to the shallow water table the hole quickly filled with water. Within five minutes a film of Schwimmeisen was established on the water surface. No flocculent formed in the hole during the five minutes of observation. The timeline for the transformation of Schwimmeisen to flocculent is presently unclear.

Additional observations showed that no flocculent appeared for several hours after the film appeared. It is likely that longer than 6 hours is necessary for the flocculent to form at the bottom of the seep pools, i.e. at least twice as long as the duration of the negative observation time of several hours. It is possible that rain or cold temperatures could alter the reaction time of Schwimmeisen converting to flocculent.

Formation of Ferrihydrite

Cornell and Schwertmann (2003) describe ferrihydrite as a common initial phase in the formation of iron oxides. They find that it forms wherever Fe(II) containing waters appear at or near the aerated surface. Under these conditions ferrous iron is oxidized abioitcally at a very high rate, which inhibits more crystalline oxides from forming. They also state that soluble silica, which is often present in such waters, forms with or on the ferrihydrite, further retarding the transformation into more crystalline iron oxides.

Ferrihydrite may also be formed via oxidation by bacteria, specifically *Gallionella* sp. and *Leptothrix* sp.. Banfield and Zhang (2001) describe bacteria using iron in redox reactions to generate metabolic energy. In this process iron oxidation may take place where it is thermodynamically favored but kinetically inhibited by low oxygen levels. They find ferrihydrite nanoparticles aggregating into colloids or collecting directly on cell-associated polymers. These types of bacteria form part of the red-orange mineral-loaded biomass that forms at the bottom of iron rich waters.

Groundwater conditions along the Oregon Coast are conducive to ferrihydrite formation with circumneutral pH, mild temperatures, dissolved silica levels of 4.4 to 6.7 ppm, iron levels of 1.2 to 9.4 ppm, and oxidizing surface conditions. Cornell and Schwertmann (2003) specify that, under conditions similar to those mentioned above, two-line ferrihydrite abiotically oxidizes quickly, inhibiting other oxides from forming. This high rate of formation may be observed in the Schwimmeisen films forming within an hour of a heavy rainstorm, which previously had destroyed their appearance.

Ranourt et al. (2005) give seven possible mechanisms for ferrihydrite precipitation, only two of which have been observed in nature. The first of these is heterogeneous nucleation on the bacterial cell wall. The second is the abiotic precipitation of hydrous ferric oxides, which adhere to the cell walls of the bacteria. They indicate that the end product of these conditions, ferrihydrite, is essentially the same, but the conditions under which it forms are different. When iron is associated with bacteria or bacterial organic matter it acts as a strong flocculating agent in water with pH levels below 4. Schwimmeisen observed along the Oregon coast may be part of the primary steps of ferrihydrite precipitation and flocculation. Schwimmeisen may be observed without flocculants on the bottom of the pool, but flocculants, on the pool bottom are associated with the films on the pool surface. Abiotic formation of Schwimmeisen occurs at pH levels of 5 to 6 on the Oregon coast.

Along the Oregon Coast *Leptothrix* has been found in the seep pools (Johnson, 2003). Tuhela et al. (1997) indicates that oxidation is more rapidly abiotically driven at higher pHs, although *Leptothrix* can oxidize iron at pH levels above 5.0. This means that while bacteria may be present, the common iron oxidizing bacteria are not likely to be very active in the pH range of the Oregon Coast dune seeps. Tuhela et al. (1997) also found that *Gallionella* does not grow under anaerobic conditions or in the absence of a carbon source. In organic rich environments ferrihydrite is the dominant phase of precipitated iron where pH levels are around 5.0 (Bigham et al., 1992).

This study has found that ferrihydrite forms from precipitation of iron as the iron changes from ferrous to ferric state. The initial precipitation may be observed as iridescent films, Schwimmeisen, floating on the surface of the pools, which take between 5 minutes and 1 hour to form. After some time, likely at least 6 hours, part of the film oxidizes completely, it then becomes the red-orange flocculent found on the bottom of the pools. This cycle may be seen in Figure 46.

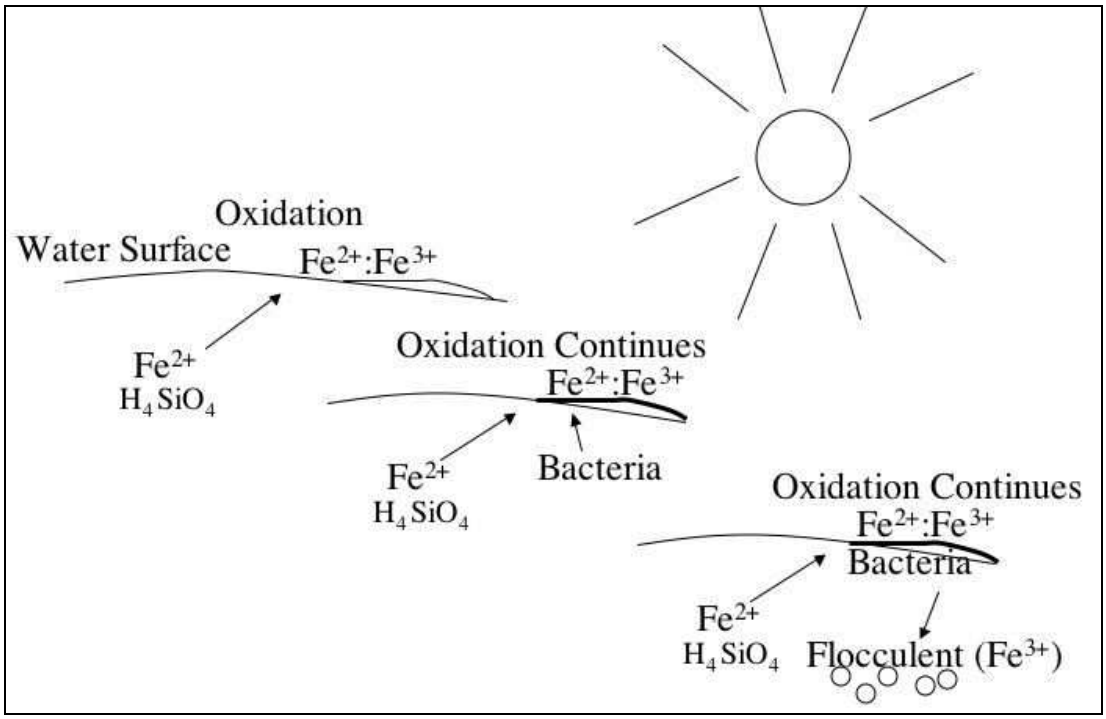

Figure 46. Cycle of formation of Schwimmeisen: initial oxidation creates the film, as oxidation continues bacteria appear, when the film is fully oxidized it falls, with the attached bacteria, to the bottom of the pool as ferrihydrite flocculent. The mixed-valent Schwimmeisen remains on the surface.

Bacteria are found in the flocculent, but not on the Schwimmeisen, suggesting that while these organisms may take advantage of the oxidation of iron they are not the direct cause of the iron precipitation. Inorganic and organic carbon are present in the system, as evidenced by water chemistry data, HRSEM, TEM and FTIR. However, the lack of carbon evidence from the TGA suggests that the carbon might not occur as a structural component of the film, or that it is in very low concentrations. If there had been a weight loss near 500 °C in the TGA analysis then one would expect carbon to be a more important part of the structure of Schwimmeisen. The exact role of carbon has not yet been constrained for this system.

Abiotic v. biotic formation (Biofilms)

As mentioned in the previous section, ferrihydrite can be precipitated either abiotically or biotically. In the iron cycle, as summarized by Emerson and Weiss (2004), Fe^{2+} oxidizes instantaneously with air or through mediation for anoxygenic photosynthesis with bacteria. Ferrous iron most commonly oxidizes spontaneously when exposed to the atmosphere or the aerobic zone in subsurface environments. Differences between abiotic and biotically formed ferric iron oxides include the presence or absence of abundant populations of bacteria cells (Emerson and Weiss, 2004).

Studies by Banfield et al. (2000), Emerson and Weiss (2004), Konhauser and Ferris (1997) and Rancourt et al. (2005) have found biotically formed ferrihydrite in environments where groundwater interacts with the surface air. These studies also found iron flocculation. Emerson and Weiss (2004) studied an iron seep associated with a wetland, where they found evidence of many sheath-like bacteria. Konhauser and Ferris (1997) studied iron oxidizing bacteria in biofilms from tropical and temperate rivers systems, as well as from metal-contaminated lake sediments. They found that bacteria scavenge metallic ions, which are then incorporated into cell walls, creating material rich in iron and often silica. In a laboratory study comparing biotic and abiotic oxide formation of ferrihydrite, Rancourt et al. (2005) used mineral magnetometry and Mössbauer analysis to find that biotic ferrihydrite is smaller in size, with weaker Fe to particle bond strength, than abiotically formed ferrihydrite. Banfield et al. (2000) suggest that crystals form because *Gallionella* and *Leptothrix*

enzymatically oxidize dissolved ferrous iron, which then becomes the lower soluble ferric phase that forms the colloidal aggregates of ferrihydrite.

Bacteria oxidize iron, and other metal ions, though interactions with reactive acidic groups contained within the bacterial cell walls and external sheaths or capsules (Konhauser and Ferris, 1997). These acidic groups are contained in polymers that act as a buffer zone between the organism and the environment, helping keep the potentially-toxic metal concentrations from accumulating in the cell. Complex microbial communities form on submerged solid surfaces and are often referred to as biofilms. These films are often submerged. Each bacterium that makes up these biofilms is roughly 500 nm thick, thicker than the Schwimmeisen found along surface of pools on the Oregon Coast. These factors, together with the rarity of bacteria cells in the iron-bearing films, lead me to conclude that Schwimmeisen is not a biofilm (Figure 15 and Figure 23).

Bacteria found in the flocculent on the bottom of the pools and in the flocculent on the Schwimmeisen film, as well as bacteria in the associated soils, may be responsible for maintaining the conditions under which Schwimmeisen forms. Emerson and Weiss (2004) specify that oxidation at the water-air boundary is the most common oxidation method, but also concede that bacteria are part of the environment where such precipitation occurs. The results of this study suggest that Schwimmeisen forms as Fe^{2+} oxidizes when it meets the atmosphere at the surface of the seep pools. As the film ages the remaining Fe^{2+} in its structure oxidizes. The fully oxidized material then sinks to the bottom of the pool as pure two-line ferrihydrite. Bacteria

live in the flocculent and may help preserve the conditions under which Schwimmeisen forms, by mediating the amount of Fe^{2+} and Fe^{3+} in the water through further oxidation and reduction (Rancourt et al., 2004).

Floating Film

Aside from the composition of Schwimmeisen, there are two points to be made about the formation of this film. The first is that Schwimmeisen is found only at the water surface, between anoxic and oxic environments. The second is that Schwimeisen stays at the surface. Upon disturbance Schwimmeisen appears to dissolve into the water. Optical microscopy indicates that it does not necessarily dissolve, but retains some of its plate like shape. Upon aging Schwimmeisen turns into the flocculent and sinks to the bottom. In its primary form it remains at the surface.

Schwimmeisen forms at the surface due to oxidation of the ferrous iron in the groundwater. The surface of the water is the most readily available source of oxygen, which then oxidizes the iron in solution. In pools that have been sitting undisturbed for some time there is Schwimmeisen and flocculent. It has been observed in the field that where the Schwimmeisen film is occurring a hole may be dug in the sand and another Schwimmeisen film will appear out of the water that has risen to the level of the water table. No time has passed that the iron at the bottom of this new pool could oxidize to form flocculent, but Schwimmeisen forms at the surface. This seems to indicate that Schwimmeisen are a precursor to the other iron phases in the system. The proposed cycle starts with the Schwimmeisen forming first, they are at the surface

and the first things oxidized, then as time passes and the Schwimmeisen fully oxidized and the flocculent begins to appear.

Schwimmeisen could also be floating on the surface of the water due to surface tension, which comes from the forces acting between water molecules (Dunkerley, 2002). These unbalanced forces allow matter to sit on the surface of the water. The surface tension at room temperature of water is 0.072 Nm^{-1} while the presence of organic matter lowers the surface tension of the water to about 0.067 Nm^{-1} (Slauenwhite and Johnson, 1996). Schwimmeisen has a density of 3.9 g/cm^3. The high densities require that Schwimmeisen floats via surface tension. A study by Tuckermann and Cammenga (2004) looked at water-soluble organic compounds, that lower the surface tension of the water. They found that low concentrations of water-soluble organic compounds, in the 0.01 – 0.1 mgC/mL range, are enough to affect the surface tension.

Some water-soluble organic compounds may be considered sea slicks. Sea slicks are coastal phenomena made up of insoluble fatty acids with more than twelve carbon atoms that form surface films at the air-water interface (Tuckermann and Cammenga, 2004). Hühnerfuss et al. (1994) give three ways in which sea slicks may be distributed and arranged: the molecules may spread homogeneously, the molecules may form “islands” ranging from several microns to several hundred microns across, or the group structure may vary in dependence on the hydration-dehydration effects. Only a small amount of carbon is needed for some films to float.

The amount of carbon in Schwimmeisen has not been constrained. It may be structural or a contaminant. TEM element mapping indicates that the majority of the carbon observed in the film is in a different plane than the Schwimmeisen. This indicates that the majority of the carbon is adsorbed onto the Schwimmeisen or was present as a slick.

Future Work

Completion of this project leads to several suggestions on future work dealing with Schwimmeisen. Foremost is the synthesis of the film. By reproducing Schwimmeisen in controlled settings the role of silica, carbon and bacteria will be constrained and their importance to the formation and structure of the film resolved.

The amount of change Schwimmeisen goes through between sample collection and analysis could be determined through a field laboratory. Samples that were not placed in a closed environment were exposed to an oxic environment for at least four hours before analysis began. A field laboratory could constrain what changes occur over this time.

Additional analytical methods would provide more details about the characterization of Schwimmeisen. Mössbauer was not possible due to the quantity of film needed for analysis, but in the future could provide more information on the crystal structure. Microprobe analysis was attempted, but unsuccessful due to the lightweight nature of the film and the inability to pin it to a sample holder. Future

work will hopefully find better ways of collecting Schwimmeisen so that more complete analyses may be made.

CONCLUSIONS

In this study along the Oregon Coast Schwimmeisen films were found to be a mixed-valent Fe/Si hydroxide mineral found in quiescent seep pools at Driftwood Creek Wayside and Seal Rock State Park. Similar films have been observed around the world, but this is only the second naturally occurring mixed-valent mineral, leading to a unique name. The seep water is characterized by soluble Fe^{2+} concentrations in excess of 5 ppm, low Eh values, near-neutral pH. Schwimmeisen does not form during times when the weather disturbs the water surface, such as during rain showers or times with high winds. While Schwimmeisen looks to be thin at first and may get thicker over time, an average thickness, estimated from SEM images, is between 100 and 300 nm. Upon physical disturbance Schwimmeisen breaks up into plates or appears to dissolve into the water. Optical microscopy indicates that it does not break up completely, but remains suspended in the water column.

Schwimmeisen is a mixed-valent nanocrystallline material with some silica incorporated into the structure. The Fe(II) to Fe(III) ratio is 1:5 while the silica to iron ratio is 1:2 at Seal Rock and 1:3 at Driftwood Creek Wayside. Schwimmeisen contains two-line ferrihydrite peaks, as well as a 4.5Å line is found in some parts of the film, but not all. Other peaks at 1.63 Å, between 1.57 - 1.56 Å, 1.45 Å, and between 1.33-1.32 Å are also found in XRD patterns. FTIR analysis indicates there are OH bonds consistent with ferrihydrite. XRD and FTIR both show evidence of the silica. Schwimmeisen has a chemical formula of $Fe^{2+}_{0.43}Fe^{3+}_{1.72}(OH)_6$.

SEM and optical microscopy indicate that Schwimmeisen retains its platy nature after collection. In places it seems to break up in over lapping shards, while in others it has a low topography. In some areas stringy masses that are similar to the flocculent found on the bottom of the pools are found. These flocculent masses are the weathering product of Schwimmeisen, an intermediate stage between the film at the pool surface and the ferrihydrite flocculent on the bottom of the pool.

Carbon is present in the pool, as well as on the Schwimmeisen. HRSEM and TEM analysis indicate that there is carbon on Schwimmeisen, although the role it plays is still unclear. Some carbon may adhere to the substrate the Schwimmeisen is being collected on, thus incorporating it into some of the analytical methods. TGA analysis does not indicate a drop at 500 °C, adding further evidence for the lack of carbon in Schwimmeisen. Similarly, bacteria are not found in conjunction with Schwimmeisen, although iron-oxidizing bacteria such as *Leptothrix* are found in the flocculent on the bottom of the seep pools where Schwimmeisen are found. No bacteria were found in Schwimmeisen itself. The transition to flocculent might also be a largely abiotic process in the observed seep pools. It was determined that Schwimmeisen forms abiotically via rapid oxidation of Fe^{2+} at the air-water boundary.

REFERENCES

Acworth, I., Jankowski, J., Turner, I, and Soriano, R., 1998, Interaction Among Coastal Sand-Dune Aquifers, Adjacent Wetlands and Seawater, New South Wales, Australia *in* Brahana, J.V., Eckstein, Y., Ongley, L.K., Schnider, R., and Moorse, J.E., eds., Proceedings of the Joint Meeting of the XXVIII Congress of the International Association of Hydrogeologists and the Annual Meeting of the American Institute of Hydrologists on Gambling with Groundwater – Physical, Chemical, and Biological Aspects of Aquifer – Stream Relations, 28, p. 461-468.

Banfield, J.F. and Navrotsky, A., 2001, Nanoparticles and the Environment: Reviews in Mineralogy and Geochemistry, Mineralogical Society of America, v. 44, p. 349.

Banfield, J.F., Welch, S.A., Zhang, H., Ebert, T.T., and Penn, R.L., 2000, Aggregation-based crystal growth and microstructure development in natural iron oxihydroxide biomineralization products: Science, v. 289, p. 751-754.

Banfield, J.F., and Zhang H., 2001, Nanoparticles in the Environment, *in* Banfield, J.F. and Navrotsky, A., 2001, Nanoparticles and the Environment, Reviews in Mineralogy and Geochemistry, Mineralogical Society of America, v. 44. p. 1-58.

Barthelmy, D., 2005, Mineralogy Database: Ferrihydrite, http://www.webmineral.com/data/Ferrihydrite.shtml, Webpage accessed June 2004 through August 2005.

Benner, S.G, Hansel, C.M., Wielinga, B.W., Bostick, B.C., Barber, T., and Fendorf, S.E., 2002, Reductive dissolution and biomineralization of iron oxides under dynamic flow conditions: Environmental Science and Tehnology, 36, no. 8, p. 1705-1711.

Bernal, J.D., Dasgupta, D.R., and Mackay, A.L., 1959, The Oxides and Hydroxides of Iron and Their Structural Inter-Relationships: Clay Minerals, v. 4, p. 15-29.

Bigham, J.M., Schwertmann, U., and Carlson, L., 1992, Mineralogy of precipitates formed by the biogeochemical oxidation of Fe(II) in mine drainage, *in* Skinner, H.C.W., and Fitzpatrick, R.W., eds., Biomineralization: Processes of iron and Manganese Modern and Ancient Environments, Catena Supplement 21, Germany, p. 219-232.

Brown, S.G. and Newcomb, R.C., 1963, Groundwater resources of the coastal sand-dune area north of Coos Bay, Oregon: U.S. Geological Survey Water-Supply Paper 1619-D.

Campbell, A.S., Schwertmann, U., Stanjek, H., Friedl, J., Kyek, A., and Campbell, P.A., 2002, Si Incorporation into Hematite by Heating Si-Ferrihydrite: Langmuir, v. 18, p. 7804 – 7809.

Campbell, E.E. and Bate, G.C., 1998, Tide-induced pulsing of nutrient discharge from an unconfined aquifer in to an *Anaulus australis*-dominated surf-zone: Water SA, v. 24, no. 4, p. 365-370.

Clough, C.M., 2005, Geologic model and geotechnical properties of stratified paleodune deposits, central Oregon coast, Oregon [M.S. thesis]: Portland, Oregon, Portland State University 148 p.

Cooper, Jr., H.H., 1959, A Hypothesis Concerning the Dynamic Balance of Fresh Water and Salt Water in a Coastal Aquifer: Journal of Geophysical Research, v. 64, no. 4, p. 461-467.

Cornell, R.M. and Schwertmann, U., 2003, The Iron Oxides: Structure, Properties, Reactions, Occurrences and Uses: Wiley-VCH, Weinheim, Germany, 664 p.

Dunkerley, D., 2002, Surface tension and friction coefficients in shallow, laminar overland flows through organic litter: Earth Science Processes and Landforms, v. 27, no. 1, p. 45-58.

Emerson, D., and Weiss, J.V., 2004, Bacterial Iron Oxidation in Circumneutral Freshwater Habitats: Findings from the Field and the Laboratory: Geomicrobiology Journal, v. 21, p. 405-414.

Frank, F.J., 1970, Ground Water Resources of the Clatsop Plains Sand Dune Area, Clatsop County, Oregon: U.S. Geological Survey Water-Supply Paper 1899-A.

Gamer, R.L., 1974, The Oregon Coast From Seal Rock to Haceta Head: Geological Newsletter: Geological Society of the Oregon Country, v. 40, no. 9, p. 65.

Grathoff, G.H., Baham, J., and Peterson, C.D., 2003, Al, Fe, Si Minerals in Dunal Soils Near Newport, Oregon, USA: Euroclay 2003 10th Conference of the European Clay Groups Association, Abstracts, Modena, Italy, June 22-26, 2003, p. 118.

Grathoff, G.H., Peterson, C.D., and Beckstrand, D.L., 2001, Coastal Dune Soils in Oregon, USA, forming allophane, imogolite and gibbsite 2001: A Clay Odyssey, Proceedings of the 12th International Clay Conference, Bahia Blanca, Argentina, July 22-28, 2001, p. 197-204.

Hart, R. and Peterson, C., 1997, Episodically buried forests in the Oregon surf zone: Oregon Geology, v. 59, no. 6, p. 131-144.

Hühnerfuss, H., Fericke, A., Alpers, W., Thesi, R., Wismann, V., and Lange, P., 1994, Classification of sea slicks by multi-frequency radar techniques: new chemical insights and their geophysical implications: Journal of Geophysical Research, v. 99 (C5), p. 9835-9845.

Johnson, C.M., 2003, Iron mineralogy in the Newport Dune Sheet Oregon Coast: [B.S. Honors Thesis], Portland, Oregon, Portland State University, 37 p.

Johnson, K., Moore, K., Smith, W., 2002, Workshop Highlights Iron Dynamics in Ocean Carbon Cycle: EOS, v. 83, p. 482.

Konhauser, K.O., and Ferris, G., 1997, Bacterial Formation of Clay Phases In Freshwater Biofilms: The Dynamic Geosphere, New Delhi, Allied Publishers, p. 200-215.

Loeppert, R.L, and Inskeep, W.P., 1996, Iron, *in* D.L. Sparks, ed. Methods of Soil Analysis, Part 3, American Soc. Agron., Madison, WI, p. 639-664..

Magaritz, M., and Luzier, J.E., 1985, Water-rock interactions and seawater-freshwater mixing effects in the coastal dunes aquifer, Coos Bay, Oregon: Geochimica et Cosmochimica Acta, v. 49, p. 2515-2525.

Miyamoto, H., 1976, The magnetic properties of $Fe(OH)_2$: Material Research Bulletin, v. 11, p. 329-336.

Moore, D.M. and Reynolds, R.C., 1997, X-Ray Diffraction and the Identification and Analysis of Clay Minerals: Oxford University Press Inc., New York, 378 p.

Nagai, K., Islam, A. R., and Tazaki, K., 2001, Bacterial Fe-As mineralization: The Science Reports of the Kanazawa University, v. 46, no. 1-2, p. 49-68.

Oregon Water Resources Department, 2005, Well Log Query Application, http://stamp.wrd.state.or.us/apps/gw/well_log/well_log.php, Webpage accessed February 2005 through June 2005.

Peterson, C.D., and Hart, R., 2003, Quaternary History of the Dunes Cover the Bandon Marine Terraces: Final Report Submitted to Department of Land Conservation and Development, Salem, Oregon.

Peterson, C.D., Stock, E., Cloyd, C., Beckstrand, D., Clough, C., Eriandson, J.M., Hart, R., Murillo, J., Percy, D., Price, D., Reckendorf, F., and Vanderburgh, S., 2005, Dating and Morphostratigraphy of Coastal Dune Sheets from the Central West Coast of North America: Oregon Sea Grant Publications, Corvallis, Oregon.

Rancourt, D.G., Thibault, P.J., Mavrocordatos, D., and Lamarche, G., 2005, Hydrous ferric oxide precipitation in the presence of nonmetabolizing bacteria: Constraints on the mechanism of a biotic effect: Geochimica et Cosmochimica Acta, v. 69, no. 3, p. 553-557.

Schwertmann, U. and Friedl, J., 1998, Thin iron oxide films on pebbles in ferriferous streams: Neues Jahrbuch Fur Mineralogie, no. 2, p. 63-67.

Seehra, M.S., Raman, R.A., and Manivannan, A., 2004, Structural investigations of synthetic ferrihydrite nanoparticles doped with Si: Solid State Communications v. 130, p. 597-601.

Sheehan, K.B., Patterson, D.J., Dicks, B.L., and Henson, J.M., 2005, Seen and Unseen: Discovering the Microbes of Yellowstone: A Falcon Guide, Montana State University, Helena, Montana 128 p.

Skinner, H.C.W., and Fitzpatrick, R.W., 1992, Iron and manganese biomineralization, *in* Skinner, H.C.W., and Fitzpatrick, R.W., eds., Biomineralization: Processes of iron and Manganese Modern and Ancient Environments, Catena Supplement 21, Germany, p. 1-6.

Slauenwhite, D.E., and Johnson, B.D., 1996, Effect of organic matter on bubble surface tension: Journal of Geophysical Research, v. 101, no. C2, p. 3769-3774.

Slaughter, T.H., 1962, Beach-area water supplies between Ocean City, Maryland, and Rehoboth Beach, Delaware: U.S. Geological Survey Water-Supply Paper 1619-T.

Taylor, G., 2005, Climate of Lincoln County, Special Report, http://www.ocs.oregonstate.edu/county_climate/Lincoln_files/Lincoln.html, Webpage accessed August 2005.

Tazaki, K., Asada, R., and Ikeda, Y., 2002, Quick Occurrence of Fe-rich Biofilms on the Water Surface: Journal of the Clay Science Society of Japan, v.. 42, no. 1, p. 21-36.

Thomas, B.E., 1995, Ground-water Flow and Water Quality in the Sand Aquifer of Long Beach Peninsula, Washington: U.S. Geological Survey Water-Resources Investigations Report 95-4026, 94 p.

Tinholt, M.J. and Wendling, G.R., 1997, Descriptive Analysis of Iron Fouling in Groundwater Treatment Systems, In Situ and On-Site Bioremediation: Paper from the Fourth International In Situ and On-Site Bioremediation Symposium, New Orleans, April 28- May 1, 1997, v. 4, p. 29-33.

Tuckermann, R., and Cammenga, H.K., 2004, The surface tension of aqueous solutions of some atmospheric water-soluble organic compounds: Atmospheric Environment, v. 38, p 6135-6138.

Tuhela, Carlson, and Tuovinen, 1997, Biogeochemical transformations of Fe and Mn in oxic groundwater and well water environments: Journal of Environmental Science and Health. Part A, Environmental science and engineering, v. 32, no. 2, p. 407-426.

Vempati, R.K., and Loeppert, R.H., 1986, Influence of structural and adsorbed Si on the transformation of synthetic ferrihydrite: Clays and Clay Mineral v. 37, no. 3 p. 273-279.

APPENDIX A: SEM-EDS LOCATIONS

Seal Rock
Sample 3 (Label S3)

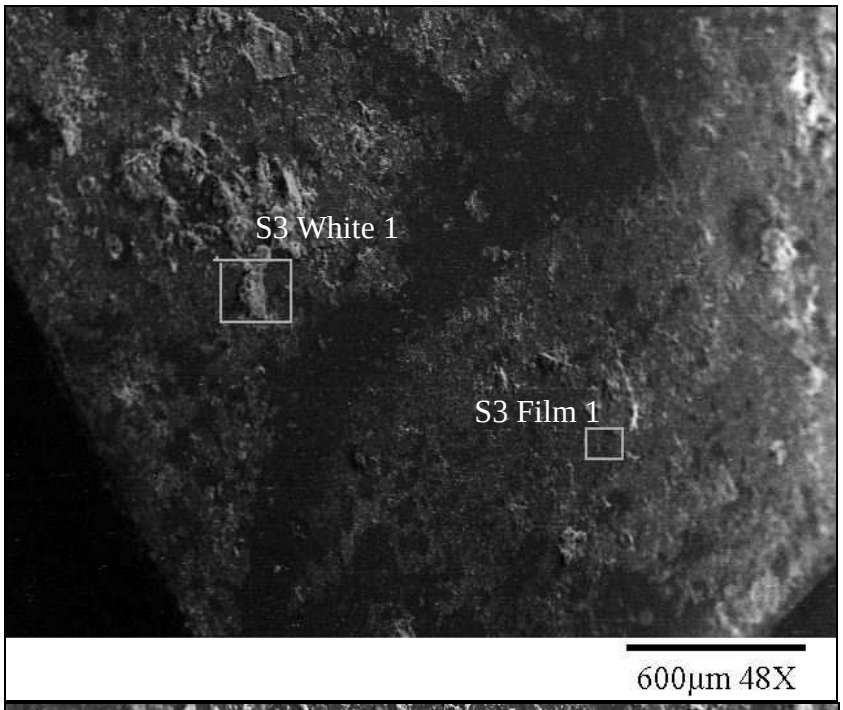

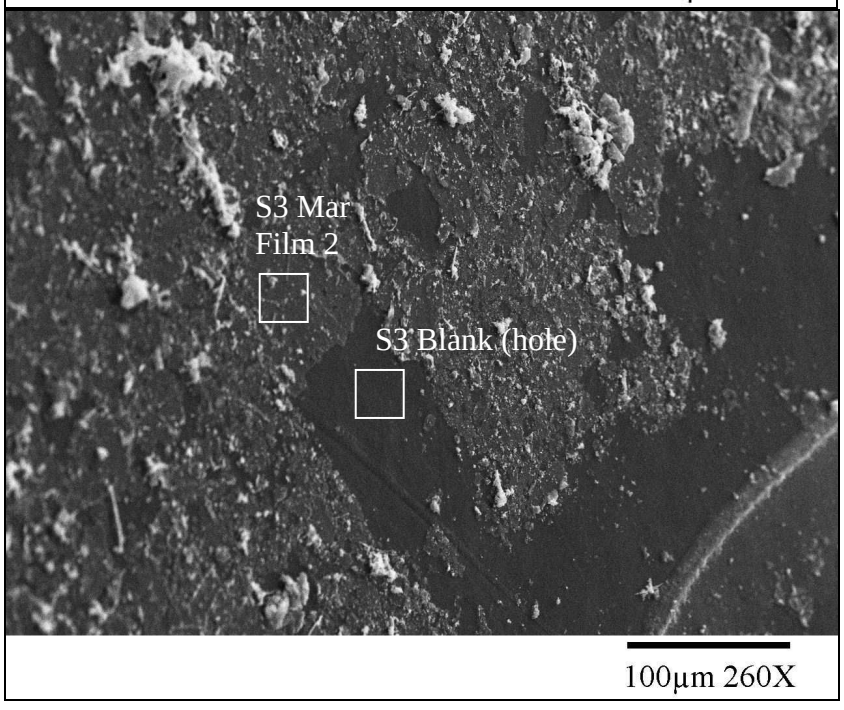

Sample 4 (Label S4)

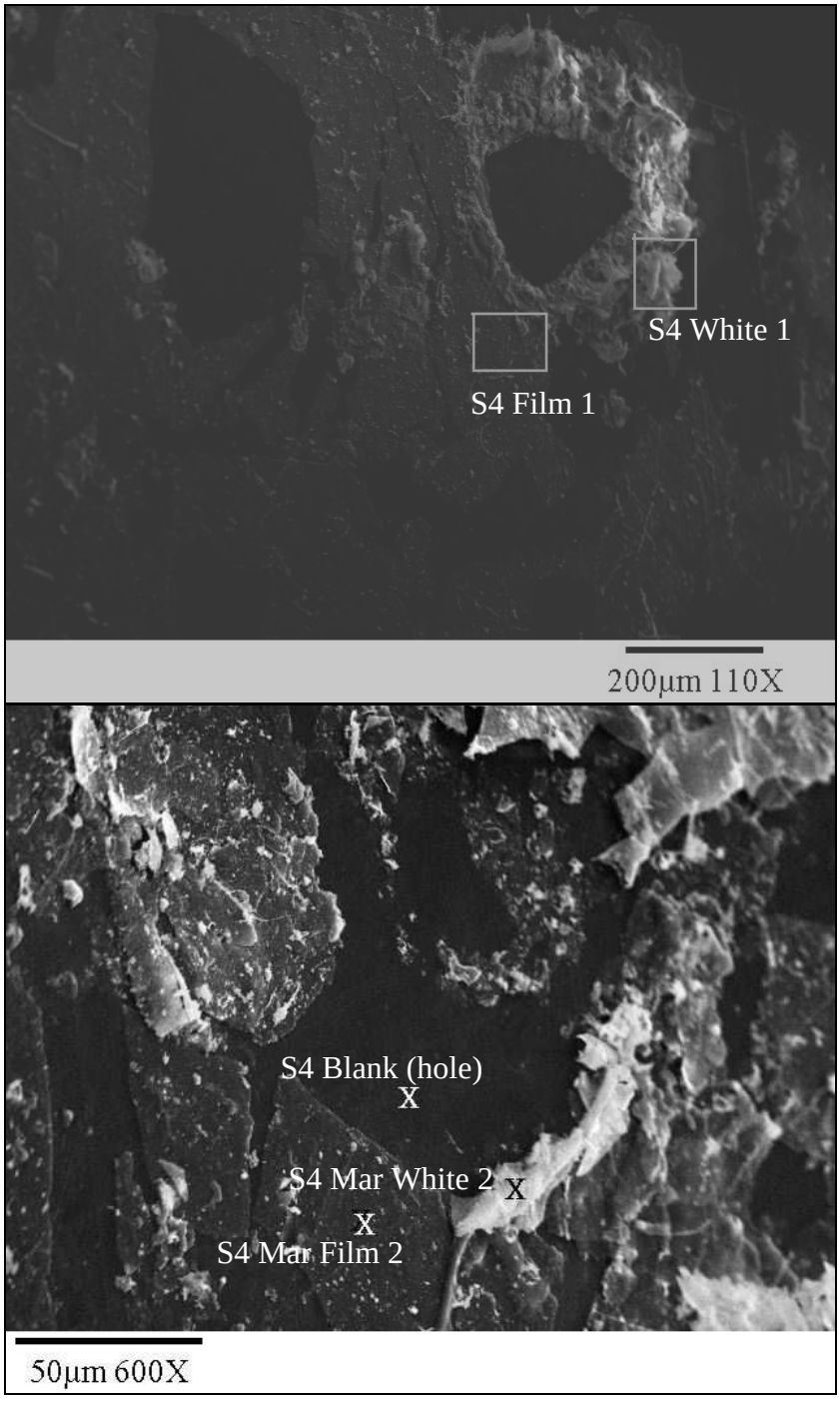

Driftwood Creek
Sample 3 (Label D3)

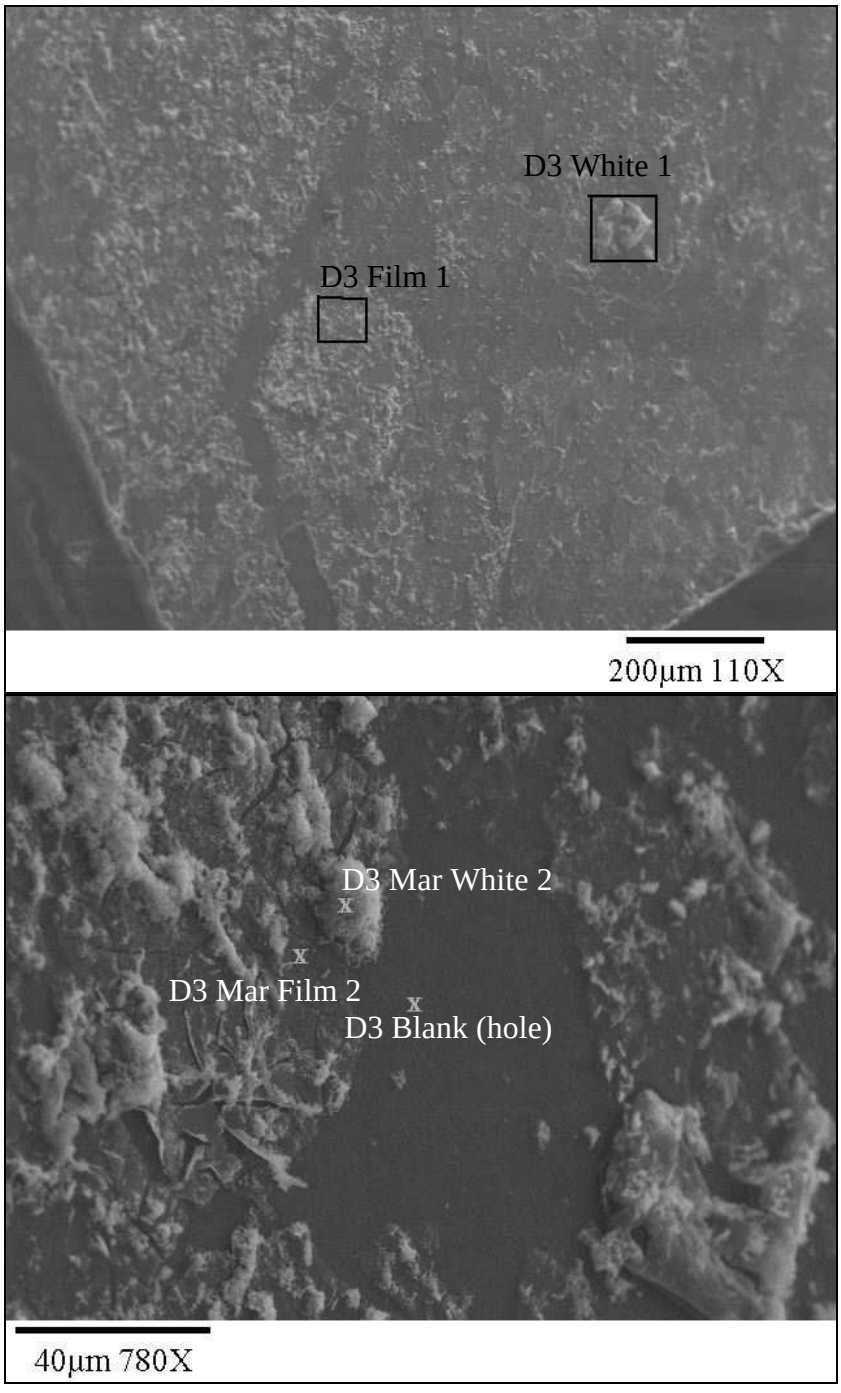

Sample 4 (Label D4)